THESIS FOR THE DEGREE OF DOCTOR OF PHILOSOPHY

Gyrokinetic simulations of microturbulence and transport in tokamak plasmas

Daniel Tegnered

CHALMERS

Department of Earth and Space Sciences
Chalmers University of Technology
Göteborg, Sweden, 2017

Gyrokinetic simulations of microturbulence and transport in tokamak plasmas
Daniel Tegnered

ISBN 978-91-7597-560-3
Doktorsavhandlingar vid Chalmers tekniska högskola
Ny serie nr 4241
ISSN 0346-718X

Department of Earth and Space Sciences
Chalmers University of Technology
SE-412 96 Gothenburg
Sweden
Telephone +46 31 772 1000

Cover:
The image shows fluctuations in electrostatic potential at three different time points.

Printed in Sweden by
Chalmers Reproservice
Göteborg, Sweden, 2017

GYROKINETIC SIMULATIONS OF MICROTURBULENCE AND TRANSPORT IN TOKAMAK PLASMAS

Daniel Tegnered
Department of Earth and Space Sciences
Chalmers University of Technology

Abstract

Fusion power is one of few viable and sustainable means of energy production. The tokamak is arguable the most mature technology to magnetically confine fusion plasmas. In these devices, heat and particle transport is dominated by small-scale turbulent fluctuations. Using high performance computing resources these phenomena can be studied in detail through numerical experiments.

The Joint European Torus (JET) is currently the largest tokamak in operation. Recently, the plasma facing components of JET were changed from carbon to metal — beryllium and tungsten. This in order to better align with the design foreseen for ITER, a next-generation device under construction in Cadarache in France. With this new wall, new impurities were introduced into the plasma. Impurities, any ion that is not a reactant in the fusion reactions, are detrimental to the fusion power as they dilute the plasma and can radiate energy. It is therefore important to study the transport of impurities and how it is affected by different operational parameters. The change of wall material has also led to a degradation in energy confinement for certain types of discharges at JET. Energy confinement must be optimized in future fusion devices for them to be economically viable. Another important issue for ITER is the refuelling of the plasma through pellet injection. The frozen hydrogen pellets are injected at high speed into the plasma. When they ablate, they perturb the density and temperature profiles. This changes the properties of the microturbulence which might hinder the particles from reaching the core of the plasma.

The present thesis aims at an improved understanding of these urgent issues by means of gyrokinetic simulations of particle and heat transport driven by Ion Temperature Gradient (ITG) and Trapped Electron (TE) mode turbulence.

Keywords: fusion, plasma physics, tokamak, turbulence, transport, impurities, gyrokinetics, Joint European Torus, ITG, TEM

List of appended papers

[A] A. Skyman, D. Tegnered, H. Nordman, P. Strand. Gyrokinetic modelling of stationary electron and impurity profiles in tokamaks. *Physics of Plasmas*, 21(9):092305, 2014.

[B] D. Tegnered, P. Strand, H. Nordman, C. Giroud, Hyun-Tae Kim et al. Comparative gyrokinetic analysis of JET baseline H-mode core plasmas with carbon wall and ITER-like wall. *Plasma Physics and Controlled Fusion*, 58(4):045021, 2016.

[C] D. Tegnered, M. Oberparleiter, H. Nordman, P. Strand, L. Garzotti, I. Lupelli et al. Gyrokinetic simulations of particle transport in pellet fuelled JET discharges. *Submitted to Plasma Physics and Controlled Fusion.*

[D] D. Tegnered, M. Oberparleiter, P. Strand, H. Nordman. Impact of a hollow density profile on turbulent particle fluxes: gyrokinetic and fluid simulations. *Submitted to Physics of Plasmas.*

Other contributions

[E] L. Fazendeiro, A. Skyman, D. Tegnered, H. Nordman, P. Strand, and J. Anderson. Gyrokinetic simulations of turbulent transport in JET-like plasmas. In *Proceedings of 40th EPS Conference on Plasma Physics, Europhysics Conference Abstracts*, 2013.

[F] D. Tegnered, P. Strand, H. Nordman, L. Fazendeiro, and A. Skyman. Predictive simulations of impurity transport at JET. In *Proceedings of 40th EPS Conference on Plasma Physics, Europhysics Conference Abstracts*, 2013.

[G] D. Tegnered, A. Skyman, H. Nordman, and P. Strand. Gyrokinetic modelling of stationary electron and impurity profiles in tokamaks. In *Proceedings of 41st EPS Conference on Plasma Physics, Europhysics Conference Abstracts*, 2014.

[H] D. Tegnered, P. Strand, H. Nordman, C. Giroud, Hyun-Tae Kim, et al. Gyrokinetic modelling of baseline H-mode JET plasmas with C Wall and ITER-like wall. In *Proceedings of 42nd EPS Conference on Plasma Physics, Europhysics Conference Abstracts*, 2015.

[I] D. Tegnered, H. Nordman, M. Oberparleiter, P. Strand, L. Garzotti, I. Lupelli et al. Gyrokinetic simulations of transport in pellet fuelled discharges at JET. *In Proceedings of 43rd EPS Conference on Plasma Physics, Europhysics Conference Abstracts*, 2016.

[J] D. Tegnered, M. Oberparleiter, H. Nordman, P. Strand. Fluid and gyrokinetic modelling of particle transport in plasmas with hollow density profiles. *Journal of Physics: Conference Series. Vol. 775. No. 1. IOP Publishing,* 2016.

Contents

Acknowledgements

I would like to express my sincerest gratitude to my supervisor Dr. Pär Strand for his constant support and encouragement. An equally huge thank you to professor Hans Nordman for always being available and providing copious amounts of helpful comments and good advice. Further, I am grateful to Dr. Andreas Skyman for helping me getting started in the world of fusion and gyrokinetics. I want to thank all the members of the group, past and current, for both useful and not so useful discussions, and the GENE team for developing this nice piece of software and providing support.

Finally, to Maj, family and friends, thank you for unwavering moral support, you are all an inspiration to me.

Chapter 1

Introduction

1.1 Nuclear fusion

Nuclear fusion is the most common energy source in the universe as it powers the stars. Two light nuclei collide and fuse into a heavier element. Without this process there would be no elements heavier than hydrogen. The mass of these new elements is not simply the mass of the reactants — it turns out that mass has been lost in the form of energy. The fact that mass can be equated with energy is known from Einstein's famous formula $E = mc^2$, where c is the speed of light in vacuum. The energy lost is equal to the nuclear binding energy as it has to be supplied in order for the reactants to separate. The larger the binding energy per nucleon, the more stable the element.

As can be seen in figure 1.1 the binding energy per nucleon is the largest for an isotope of iron, ^{56}Fe. Thus, energy is released when either elements lighter than iron are fused together or when elements heavier than iron are split, as is the case in fission power plants. The masses involved in each reaction are much larger than in chemical reactions so the fuel needed per unit of energy is much lower. However, if you want to fuse two nuclei, a new problem presents itself as the nuclei will repel each other since they are positively charged. That means that large kinetic energies and thus temperatures are needed in order to overcome this Coulomb repulsion. The energy needed to overcome the repulsion for two hydrogen nuclei is around 0.4 MeV, corresponding to a temperature of $3 \cdot 10^9$ K. Hence, nuclear fusion would be almost impossible without quantum tunnelling, which lowers the needed temperature by at least an order of magnitude.

Large temperatures mean that the matter will be ionized, since the frequency of ionizing collisions will be higher than the frequency of the recombining collisions — it can thus be in the plasma state. The important problem in fusion science is how to confine this hot plasma so that the fusion reactions can occur without too much energy escaping the system. In the stars, the plasma is gravitationally confined. The mass is large enough so that the

gravitational forces contain the plasma and the proton-proton chain reaction can occur whereby helium-4 is created from protons in multiple steps. The masses and power densities involved are such that this approach is not feasible on Earth.[1]

Another method is to bombard a small pellet of hydrogen with lasers that will compress the matter so fast that the inertia will be enough for fusion reactions to occur before the material is scattered. This method is called inertial confinement fusion. There have been high profile experiments in this area, first and foremost the National Ignition Facility, but the results are thus far disappointing [2].

A third way to confine the plasma is to use the fact that the particles of the plasma, the ions and electrons, are charged and will be subject to the Lorentz force, $\mathbf{F} = e\mathbf{v} \times \mathbf{B}$, where $\mathbf{F}$ is the force on a particle, e is the charge of the particle and $\mathbf{B}$ is the magnetic field. In absence of collisions, they will follow and circle around the magnetic field lines. This method to confine the plasma is called magnetic confinement. The magnetic confinement will be optimized if the topology of the magnetic field is such that the field lines have no endings, so that end losses can be avoided. One such topology in three dimensions is a torus. Several different schemes to use a toroidally shaped magnetized plasma have been devised, that first and foremost differ in the way the magnetic fields are created, for example the so called stellerator and the tokamak[2]. The tokamak is considered the most mature technology.

The fusion reaction that is the likeliest to occur, i.e. has the largest cross section at lower temperatures, is not the proton-proton chain of the Sun. Instead, it is the reaction between two isotopes of hydrogen, deuterium and tritium. The reaction foreseen in future first generation fusion power plants is then $\mathrm{D} + \mathrm{T} \rightarrow {}^4\mathrm{He} + \mathrm{n} + 17.6\,\mathrm{MeV}$. Five nuclei are involved in the reaction, so 3.5 MeV is released per nucleon. As a comparison, 0.85 MeV is released per nucleon during the fission of U235 and the energy released from burning one molecule of ethanol is just 13.47 eV. The neutron will not be confined by the magnetic field as it is uncharged and will leave the plasma and heat the wall. The charged helium nucleus, the so-called α-particle, on the other hand, will be confined by the magnetic field and serve to heat the rest of the plasma.

1.2 Sustainability

The world energy use in 2012 was around 17 TWy [5]. The UN reference case growth for energy demand until 2030 is $3.6 - 4.9$ TWy, mostly in the lower-middle income part of the world. Meanwhile, the energy efficiency opportunity is just $2.7 - 3.3$ TWy, mostly in the high income part of the world [6]. Given a growing global population and an increase in living standards in the third

[1] In our Sun the power density of the core is comparable to that of a compost heap [1]

[2] Formed from the Russian words **to**roidalnaya **ka**mera and **ma**gnitnaya **k**atushka, meaning 'toroidal chamber' and 'magnetic coil' [3]

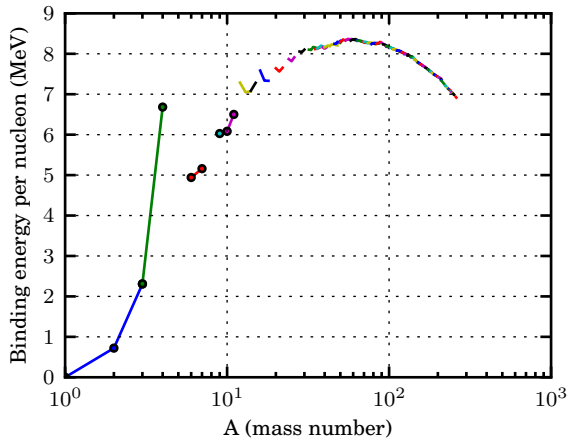

Figure 1.1: Binding energies per nucleon of the most common isotopes, connected isotopes are the same element. The binding energy is the energy that would have to be supplied in order to separate all the nucleons. Data from [4].

world, it then seems unlikely that the world energy demand will decrease in the foreseeable future.

Currently, 82 % of that energy comes from fossil fuels [7]. Fossil fuels are undesirable and unsustainable for a number of reasons, first and foremost in that their release will trigger serious climate change [8]. The finite fossil fuels are also the basis for a multitude of chemical and pharmaceutical products that we must have access to in the future. The list of energy sources that could replace the fossil fuels is however not very long: nuclear fission and fusion and renewable sources like wind and solar power. Tens of terawatts worth of production of these energy sources thus need to be constructed during the coming decades. This might be the single most daunting sustainability challenge that the world currently faces [9].

Renewable energy sources will surely play an important role in the energy mix of the future, but they are not without drawbacks. They can be of limited potential, like hydro power, which prevents them from contributing significantly. Most are very diffuse with a low energy output per unit area. Wind power, for example, has a potential of $2 - 3\,\mathrm{W/m^2}$ [10], 20 TW of power production would thus require roughly 15 times the area of Sweden. The energy and materials required to construct the energy facilities would also be significant, so a life cycle analysis approach is important. Photovoltaic systems require $11 - 40$ times more copper than fossil generation and wind power demands $6 - 14$ times more iron. In order to build a low-carbon energy system by 2050 two years of copper and one year of iron production is needed [11]. The intermittency of many of the renewable energy sources will also require

large investments in so called smart grids and energy storage solutions, this can cost as much as 1 trillion Euros up to 2030 for the European Union alone [12]. Furthermore, even though renewable energy often has a comparable price to fossil based alternatives, it has yet to make a considerable contribution to the energy mix.

Fission power also has its fair share of problems but could be developed to mitigate most of them. In 2005 there was an installed fission power capacity of 369 GW requiring 67 320 tons of uranium annually with estimated total world resources of 4 743 000 tons uranium [13]. With 20 TW of fission power production the resources would thus last only 1.3 years with present technology. At those production levels, the waste would also be a huge problem. Fourth generation breeder reactors could make use of the uranium much more efficiently, reducing the need by a factor 30 or more. However, the safety aspect, nuclear proliferation and negative public opinion are other obstacles for widespread fission power.

The fact that both renewable energy sources and fission power have failed to make an impact on the energy mix may be due to a number of lock-in mechanisms that act as barriers to diffusion of these technologies. These lock-in mechanisms can be technological in nature. The huge infrastructures that already exist, like petrol stations and natural gas pipe lines, are one such example. They can also be institutional, fossil fuel industries are subsidised to the tune of $200 billion annually [14]. In order to overcome this status quo, new strong policies are needed from the governments worldwide, but history has shown that the most efficient way of breaking such a techno-institutional complex is with a new transformative technology [14]. Nuclear fusion could be that technology.

The fuel for future fusion reactors will be deuterium and tritium. Deuterium can be obtained from so-called heavy water through electrolysis. Heavy water is obtained from fresh water through the GS isotopic exchange process [15]. The potential deuterium reserves are vast, 1 part in 6400 in water. Tritium, on the other hand, has a half-life of 12.3 years and is thus not available in nature, but must be produced at the reactor. The intention is to breed the necessary tritium from lithium-6 and the neutron from the fusion reaction in a so-called blanket in the reactor wall. The reaction is $^{6}\mathrm{Li} + \mathrm{n} \rightarrow ^{4}\mathrm{He} + \mathrm{T} + 4.8\,\mathrm{MeV}$. Consequently, the sources of fuel for a future fusion reactor will be water and lithium, with the latter being the only possible limiting factor. There are around 40 million tons of lithium available worldwide [16]. The energy content of natural lithium, using the reactions described above, is around 0.86 GWy/ton [17]. Thus, 20 TW of energy production would use 23 000 tons of lithium per year and the reserves would last in the order of 2000 years. This can be regarded as a long enough time span for the technology to be seen as sustainable. Furthermore, there are considerable amounts of lithium in sea water (0.17 g per ton) that could potentially be extracted economically in the future [18]. Lithium is, however, just like oil used for a multitude of purposes so using all for energy production is not desirable. If, for example, the global automobile fleet is electrified in

the coming decades a considerable amount of lithium will be required for the batteries.

In the reaction above to breed tritium from lithium each fusion reaction only creates one neutron, which in the breeding reaction only creates one new triton. Since losses of neutrons are impossible to avoid, so called neutron multipliers will also be needed. Beryllium and lead are two materials that could serve this purpose, and they would be used up in the reactions. It is questionable whether the worldwide resources of beryllium would be enough for a fusion powered world, the situation with lead is much better with the resources lasting in the order of 100 000 years [18].

Other than resources, for nuclear fusion to be called a sustainable energy solution, it should not be a threat to human safety or the environment in general. Nuclear fusion differs greatly from nuclear fission in that the amount of fuel in the reaction chamber is just in the order of a couple of grams. Furthermore, since the reaction depends on specific, very high temperatures any operational problems would lead to the immediate termination of the reaction. This precludes run-away reactions similar to the nuclear meltdown possible in fission power plants. The fuel (lithium and deuterium) is not radioactive, neither is the end product (helium). However, tritium is radioactive and will contaminate materials in the reactor. Furthermore the neutrons from the fusion reactions will activate materials. The choice of materials used to build the reactor is therefore very important, but with the right choice the materials could be recycled in a matter of decades [17]. All in all, fusion reactors would generate activated materials on a scale similar to that of fission power plants but with much lower long term radio toxicity since there would be no spent fuel. Release of tritium in an accident is a concern since tritium could replace hydrogen and can thus contaminate biological systems. However, at most 200 g of tritium released is foreseen as a worst case scenario in the case of an accident [17]. As mentioned, the short half-life also ensures that the area will not be contaminated for long.

Chapter 2

Magnetized fusion plasmas

Plasma is often referred to as the fourth state of matter, besides solid, liquid and gas. On Earth, it is much less common than the other three states of matter. A plasma requires charged particles. One way of creating charged particles is through ionization, whereby an atom gains or loses an electron and becomes an ion. The level of ionization in a gas depends on the temperature and density of the gas. Atoms are ionized when they collide with a particle with high enough energy. At the temperatures we commonly have around us, an atom must have been accelerated to energies much higher than the average by a series of collisions. Consequently, the number of atoms in the gas that have high enough energy goes as e^{-U_i/k_BT} where U_i is the ionization energy of the gas, k_B is the Boltzmann constant and T is the temperature.[1] The ion will stay ionized until it recombines with an electron. The recombination rate will depend on the density of the electrons and go as n_e^{-1}. The degree of ionization for air at room temperature is on the order of $\frac{n_i}{n_e} \approx 10^{-122}$.

However, it is not just the level of ionization that determines whether matter is in the plasma state. What makes a plasma different from a gas is the long range Coulomb interactions possible between the charged particles. A useful definition for a plasma is thus [19]

> "A quasi-neutral gas of charged particles which exhibits collective behaviour."

In a gas with neutral particles, these will not interact until they collide, so interaction between more than two particles is uncommon. In contrast, in a plasma the motion of the charged particles will lead to electric currents that create magnetic fields and there will be electric fields caused by temporary concentrations of positive or negative particles. These fields will interact with all the other charged particles — this is the collective behaviour. Quasi-neutrality entails that any concentration of charge will be shielded out in distances that are much

[1] In fusion reactors, it is the particles of this tail in the Maxwellian distribution, replenished by scattering collisions, that will undergo fusion reactions.

smaller than the size of the plasma. This means that the charges will balance out on a macroscopic level and the quasi-neutrality condition, $n_e = \sum_j Z_j n_j$, will hold. Here, Z_j is the charge number of species j and n_j is the density of species j. In order for this to be true, the size of the plasma must be much larger than the Debye length, $L \gg \lambda_D = (\frac{\varepsilon_0 k_B T_e}{ne^2})^{1/2}$, which is a measure of the shielding distance of a charge. In order for there to be collective behaviour, the number of particles within a Debye length from a charge must be large, $N_D = \frac{4\pi n \lambda_D^3}{3} \gg 1$ and the electromagnetic forces must be more important than the hydrodynamic forces. This means that the typical plasma oscillations must be faster than the collision frequency with neutral atoms, $\omega\tau > 1$, where ω is the frequency of a plasma oscillation and τ is the mean time between collisions.

In order for a fusion power plant to be useful, it must output at least as much energy as is put in, a condition called break-even. Ignition is the point at which all external heat sources can be turned off so that the temperature can be maintained solely from the energy of the α-particles from the fusion reactions. The energy released in the fusion reaction will be divided up between the α-particle and the neutron according to the mass so that the momentum is conserved in the collision. Hence about 80 % of the energy will be deposited on the neutron and lost from the plasma. A condition for ideal ignition where the presence of impurities in the plasma is neglected is $n_e \tau_E^* T = \frac{12 k_B T^2}{\langle \sigma v \rangle E_\alpha (1+5/Q)}$, here τ_E^* is the global energy confinement time, the total thermal energy content of the plasma divided by the lost power including radiation, $\langle \sigma v \rangle$ is the velocity averaged cross section of the fusion reaction, E_α is the energy of an α-particle and Q is the ratio of the fusion power produced to the heating power supplied. This is the so-called fusion triple product. It is used to characterize the performance of a fusion device as it combines $n_e \tau_E^*$, a measure of the merit of confinement called the Lawson criterion, with the temperature, which must also be sufficiently high to optimize fusion reactivity. The fusion triple product needed for three different Q-values is shown in Figure 2.1. Break even is the point where as much fusion power is produced as is supplied, that is $Q = 1$.

With the every tokamak constructed, the fusion triple product has doubled on average every 1.8 years, faster than "Moore's law" for the number of transistors in a microprocessor [20]. The JT60U Tokamak in Japan currently holds the record for the largest fusion triple product while the Joint European Torus (JET) in the UK has produced the highest fusion power, 16 MW, which corresponded to a Q value of 0.65. The next step is the construction of ITER in Cadarache in France. The goal of ITER is to produce 500 MW of output power with a Q-value of 10 for a duration of up to 480 seconds.

2.1 The tokamak

The Lorentz force $\mathbf{F} = e\mathbf{v} \times \mathbf{B}$, makes charged particles travel in helical orbits around the magnetic field lines, here e is the charge of the particle and $\mathbf{v}$ is its velocity. The radius of the gyration, the Larmor radius, is $\rho = \frac{m v_\perp}{|e|B}$ where $v_\perp$

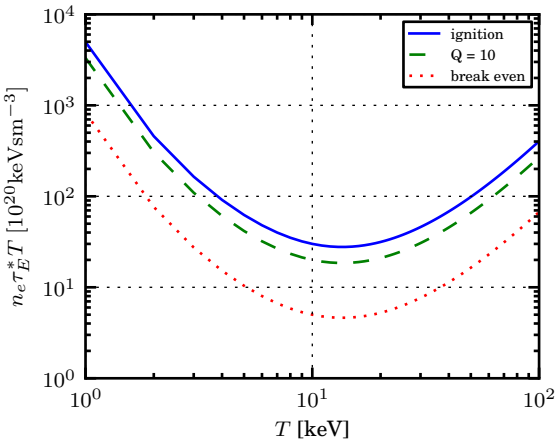

Figure 2.1: Fusion triple product versus temperature for the DT reaction, fusion cross section data from [21].

is the velocity of the particle perpendicular to the magnetic field lines. It is much smaller for the electrons than for the ions. The frequency of this gyration, the cyclotron frequency, is $\omega_c = |e|\,B/m$. Sans collisions and turbulence, the particles' guiding centres would stay tied to to the field lines but remain free to move along them. The most obvious way to avoid losses of particles at the end of the magnetic field lines is to connect them in a toroidal configuration. This toroidal field can be produced by poloidal currents in coils external to the plasma. The toroidal field will go as $B_\phi \propto \frac{1}{R}$ where R is the radial distance from the centre of the tokamak.

However, particles following the field lines in such a configuration will be subject to drifts caused by the gradient of the magnetic field strength and the curvature of the field lines. The ∇B drift is caused by the fact that the Larmor radius will be smaller where the magnetic field strength is larger. It is given by $\mathbf{v}_{\nabla B} = \frac{1}{2}\frac{mv_\perp^2}{eB}\frac{\mathbf{B}\times\nabla B}{B^2}$. The drift due to the curvature of the magnetic field lines is given by $\mathbf{v}_c = \frac{mv_\parallel^2}{eB}\frac{\mathbf{B}\times\nabla B}{B^2}$ [3]. Because of the dependence on the charge, these drifts will be in different directions for the electrons and the ions, creating a vertical electric field. This in turn will lead to an $\mathbf{E}\times\mathbf{B}$ drift according to $\mathbf{v}_E = \frac{\mathbf{E}\times\mathbf{B}}{B^2}$ that will cause both the electrons and ions to drift together, since the $\mathbf{E}\times\mathbf{B}$ drift is neither dependent on mass nor charge, radially outwards. The solution to this is to introduce a twist in the magnetic field lines by giving the field a poloidal component, B_θ. Then, the field lines will trace out nested surfaces, so-called flux surfaces. In a tokamak, the poloidal field is achieved by driving a current through the plasma. This is done by inducing a toroidal electric field by transformer action, that is, a flux change is generated through the torus. The current will then create the magnetic field through Ampere's

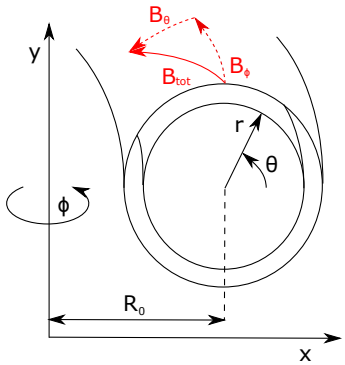

Figure 2.2: Toroidal geometry with two nested flux surfaces.

law. The helical twist then compensates the toroidal drift as particles will spend time both on the inside and the outside of the device.

The condition for equilibrium is that the force on the plasma must be zero everywhere, that is, the magnetic force must balance the force due to the plasma pressure,

$$\mathbf{j} \times \mathbf{B} = \nabla p. \tag{2.1}$$

It follows that $\mathbf{B} \cdot \nabla p = 0$ so that the flux surfaces are surfaces of constant pressure, it also follows that $\mathbf{j} \cdot \nabla p = 0$ and thus that the current lines also lie in the flux surfaces. The safety factor is a measure of how twisted the field lines are, and can be approximated as $q = \frac{rB_\phi}{R_0 B_\theta}$, where r is the radial coordinate, in the circular limit. The safety factor can differ from flux surface to flux surface, the minimum is often near the magnetic axis with an increase outwards. The measure of how much the safety factor changes from flux surface to flux surface is the magnetic shear, $\hat{s} = \frac{r}{q}\frac{dq}{dr}$. If the cross section is circular, it is determined by the toroidal current density.

In general, the magnetic geometries in tokamaks are not circular, which makes it convenient to introduce flux functions that are constant on a flux surface, instead of relying on r. One such flux function is the poloidal magnetic flux function, ψ which is determined by the poloidal flux within each flux surface [3]. Flux surfaces and the commonly used coordinate system in a toroidal geometry is shown in Figure 2.2.

The equilibrium equation, Eq. 2.1, can for an axisymmetrical plasma be written as a differential equation dependent on two arbitrary functions of the poloidal flux function, $p(\psi)$ and $f(\psi)$ as

$$R\frac{\partial}{\partial R}\frac{1}{R}\frac{\partial \psi}{\partial R} + \frac{\partial^2 \psi}{\partial z^2} = -\mu_0 R^2 p'(\psi) - \mu_0^2 f(\psi) f'(\psi),$$

where $'$ denotes the derivative with respect to the poloidal flux. This is the Grad-Shafranov equation [3]. Numerical solutions to this equation are used in

many simulation codes as well as different parametrizations. One such tokamak equilibrium model is the Miller model in which an expansion of the Grad-Shafranov equation is made, local to a flux surface, in terms of nine parameters. These parameters are the safety factor and magnetic shear, as well as the aspect ratio ($\varepsilon = r/R$), the pressure gradient (α), the elongation (κ), triangularity (δ), and the radial variation of κ, δ, and R [22]. These equilibrium parameters are important to the stability of the microturbulence. The elongation is one of the factors commonly used in the empirical scaling laws of the energy confinement time [23]. An example of a geometry featuring elongation and triangularity is shown in Figure 4.2.

2.2 Impurities

Impurities, which are here defined as any ion that is not a reactant in the fusion reaction, are detrimental to the performance of fusion devices in several ways. They dilute the plasma, lowering the output power and they can also cool the plasma through radiation. Heavy impurities might not be stripped of all their electrons. If the remaining electrons are excited, they emit photons of specific frequencies when they once again are de-excited, so called line radiation.

There are several sources of impurities in tokamaks, they might be injected for control purposes or in order to decrease the power load on the plasma facing components. Impurities can also be released through the interaction of hot particles with the wall. For this reason, tokamak walls are often coated with light elements such as carbon, or beryllium, the coating foreseen for ITER and tested with the new ITER-like wall at JET. However, the power densities at the divertor, where the magnetic field lines are in contact with the vessel, will be even higher at around $10\,\mathrm{MWm}^{-2}$, requiring materials with higher meting points such as tungsten. The third source of impurities are the fusion reactions themselves. The resulting thermalised helium must be transported out of the plasma sufficiently rapidly. How, and at what rates the impurities are transported, inwardly or outwardly, during different conditions, is thus of great importance since strong inward transport of a heavy impurity like tungsten might be lethal to the discharge. This is investigated in paper A.

2.3 The JET ITER-like wall

The current design for ITER includes a main chamber wall made from Beryllium. This is the lowest Z metal with acceptable mechanical and thermal properties. The low Z means that it is more benign as an impurity as it dilutes the plasma less and does not cause any line radiation in the core of the plasma. At the start, the plasma facing components at JET were made from carbon fibre composite (CFC), however, this material is not acceptable for the main wall of ITER because of the risk of tritium retention. In order to demonstrate the reduction in tritium retention and test the ability to operate a high power

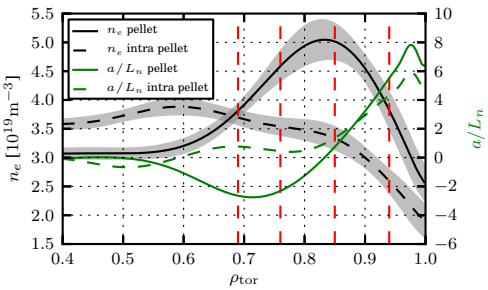

Figure 2.3: Density profiles at the time point when the effect from the pellet is the largest and when the profile has relaxed again in a pellet fuelled JET L-mode discharge. Dashed lines indicate the radial positions that were simulated nonlinearly in paper C.

tokamak within the limits set by the new materials, the ITER-like wall (ILW) was installed at JET. It comprises a main chamber wall of solid beryllium and tungsten and tungsten coated CFC for the divertor tiles [24]. The fuel retention has been demonstrated to be at least a factor 10 lower than with the C-wall [25] and that the power handling with the new materials works well [26]. However, the global energy confinement has been negatively affected by the need for increased gas fuelling in order to avoid tungsten accumulation in the core [27]. The lower confinement has been correlated to degraded confinement in the so-called pedestal, close to the edge of the plasma. This causes the temperatures to be lower in the edge which in turn changes the power deposition from the neutral beam injection (NBI) power system [28]. Whether the core confinement also is affected is the subject of Paper B.

2.4 Pellet fuelling

Pellet fuelling, whereby frozen pellets of hydrogen isotopes are injected into the plasma at high speeds, will be the primary fuelling system for the core plasma of ITER [29]. This method is energy efficient compared to neutral beam injection and it allows for better control over the plasma density than gas injection [30]. However, when the frozen pellet ablates, it will temporarily disturb the profiles of temperature and density, which might result in a local maximum as shown in Figure 2.3. This changes the microstability and transport properties of the plasma. Particularly in regions of positive density gradient, the ITG mode, as discussed in Section 3.4.1.1, has been seen to be stabilized [31]. This can have serious consequences if the turbulent particle transport, as discussed in Section 3.4, is suppressed. The pellet particles might then diffuse towards the edge rather than the core. This is explored in Papers C and D.

Chapter 3

Transport theory

In order to achieve fusion power economically, the fusion triple product, $n_e \tau_E^* T$, must be maximized, here n_e is the electron temperature, τ_E^* is the energy confinement time, and T is the temperature. However, the temperature and density are constrained respectively by the need to maximize the fusion cross-section and maintaining global stability. The stability constraint on the density is the so called Greenwald limit, an empirical result that limits the plasma density to $n/10^{20} = \kappa J$, where κ is the elongation and J is the average current density in $\mathrm{MA/m^3}$ [3]. The temperature and density are also constrained by the β limit, β is the ratio of the plasma pressure to magnetic pressure, $\beta = \frac{nT}{B^2/(2\mu_0)}$. If the plasma pressure becomes too large compared to the magnetic pressure, large scale magnetohydrodynamic instabilities, such as ballooning modes, will occur. A high β value is important from an economic standpoint since the fusion power scales as n^2 while the strength of the confining magnetic field is a large factor in the cost of the device.

Hence, the only avenue to improve the fusion triple product is to increase the energy confinement time, τ_E^*. The energy confinement time is connected to the radial transport of particles and energy from the core to the edge. The transport depends on a number of processes, from sawteeth in the centre of the plasma to edge localized modes (ELMs) towards the edge. Aside from these intermittent phenomena, the transport is determined by local processes whereby the particles undergo diffusion and convection. Diffusion is the net movement of a quantity from a region of high concentration down a concentration gradient. It can be explained by the random walk processes the particles undergo. Convection, on the other hand, is a collective movement of particles. The net convective velocity, the so-called pinch, of a species can have the opposite sign of the diffusion so that an inwardly peaked profile can be sustained in steady state.

It was long believed that the transport in tokamaks could be described by the Coulomb interactions alone as in classical and neoclassical theory. However, it was realized that the heat and particle transport observed were up to two

orders of magnitude larger [32]. The so called "anomalous" transport make up the rest and thus dominate over the neoclassical transport. It has long been accepted that turbulent transport explains this degradation in confinement. The transport can be due to instabilities that let the particles escape their flux surfaces or that lead to the break-up of the flux surfaces themselves. The main candidate for the turbulent transport is turbulence due to small scale instabilities driven by the very steep gradients in density and temperature, referred to as microinstabilities, as discussed in Section 3.4.

3.1 Kinetic approach

Collisions can be rare in high-temperature plasmas and the velocity distributions of the species might therefore remain non-Maxwellian for a long time. A kinetic description is therefore useful, describing the position and velocities of all the particles in the plasma. The dynamics can be described completely by the Newton's laws of motion and Maxwell's equations. However, with the many particles and fast time scales involved computing the motion of all the particles will be much too expensive for the foreseeable future. A statistical approach can instead be used with a distribution function for each species j in phase space, $f_j(t, \mathbf{r}, \mathbf{v})$. The kinetic energy of the particles in high temperature fusion plasmas will be much larger than the potential energy between the particles, so the particles are weekly coupled. It is then enough to take into account interactions between two particles and neglect interaction between three particles or more. The effects from the large scale fields and from those varying on the scale of a Debye length and smaller can be separated. These small scale interactions between two particles can then be treated through a separate collision operator, further described in Section 4.1. Since the collision frequency often is much lower than the frequencies of the turbulent fluctuations, the collisionless limit can be justified. Without collisions, the change of the distribution function is expected to be zero in the frame moving with the particles, $\frac{\mathrm{d}f}{\mathrm{d}t} = 0$. Writing out this total derivative for species j, we have

$$\frac{\mathrm{d}f_j}{\mathrm{d}t} = \frac{\partial f_j}{\partial t} + \frac{\partial f_j}{\partial x}\frac{\partial x}{\partial t} + \frac{\partial f_j}{\partial y}\frac{\partial y}{\partial t} + \frac{\partial f_j}{\partial z}\frac{\partial z}{\partial t} + \frac{\partial f_j}{\partial v_x}\frac{\partial v_x}{\partial t} + \frac{\partial f_j}{\partial v_y}\frac{\partial v_y}{\partial t} + \frac{\partial f_j}{\partial v_z}\frac{\partial v_z}{\partial t} = 0,$$

which can be written as

$$\frac{\partial f_j}{\partial t} + \mathbf{v} \cdot \nabla f_j + \mathbf{a} \cdot \frac{\partial f_j}{\partial \mathbf{v}} = 0.$$

With Newton's third law $\mathbf{F} = m_j \mathbf{a}$, where m_j is the mass of species j, and the force on a particle from an electromagnetic field $\mathbf{F} = q_j(\mathbf{E} + \mathbf{v} \times \mathbf{B})$, where e_j is the charge of species j and $\mathbf{E}$ and $\mathbf{B}$ are the total electric and magnetic fields, we get

$$\frac{\partial f_j}{\partial t} + \mathbf{v} \cdot \nabla f_j + \frac{e_j}{m_j}(\mathbf{E} + \mathbf{v} \times \mathbf{B}) \cdot \frac{\partial f_j}{\partial \mathbf{v}} = 0, \tag{3.1}$$

which is the Vlasov equation. However, the cumulative effect of multiple small angle collisions are often important in magnetized fusion plasmas since the range of the Coulomb interaction in principle is infinite. Adding a collision term, we get the Fokker-Planck (or Boltzmann) equation [3],

$$\frac{\partial f_j}{\partial t} + \mathbf{v} \cdot \nabla f_j + \frac{e_j}{m_j}(\mathbf{E} + \mathbf{v} \times \mathbf{B}) \cdot \frac{\partial f_j}{\partial \mathbf{v}} = \left(\frac{\partial f}{\partial t}\right)_c . \tag{3.2}$$

The collisional particle interactions are effectively random and the collision operator provides a statistical account of this. It represents the effects of soft collisions, each only making a small change in the particles' velocities [32]. In this work, the collision operator used is the linearised Landau-Boltzmann operator.

The electric and magnetic fields in Eq. 3.2 are determined by Maxwell's equations that couple back to Eq. 3.2 through the charge density ρ_j and current densities $\mathbf{j}_j$, which are obtained by taking velocity moments of the particle distribution function. Maxwell's equations,

$$\begin{aligned} \nabla \cdot \mathbf{E} &= \sum_j \frac{\rho_j}{\epsilon_0} \\ -\mu_0 \epsilon_0 \frac{\partial \mathbf{E}}{\partial t} + \nabla \times \mathbf{B} &= \sum_j \mu_0 \mathbf{j}_j \\ \nabla \cdot \mathbf{B} &= 0 \\ \nabla \times \mathbf{E} + \frac{\partial \mathbf{B}}{\partial t} &= 0 \end{aligned}$$

together with the Fokker-Planck equation completely describes a plasma self-consistently. This system is much more practical to solve than the Newton-Maxwell system. However, numerical solutions are still expensive because of the dimensionality of $f_j(t, \mathbf{r}, \mathbf{v})$ and the huge range of time scales involved, from the fast electron cyclotron frequency, to the slower frequency of the turbulent oscillation. Further simplifications are necessary; like the fluid approach where the dimensionality is reduced by three as discussed in Section 3.2 or gyrokinetic theory where the dimensionality is reduced by one, as discussed in Chapter 4.

3.2 Fluid approach

It is often enough to describe a plasma in terms of fluid quantities such as the particle density, $n(t, \mathbf{x})$, the fluid velocity, $\mathbf{u}(t, \mathbf{x})$ and the pressure, $p(t, \mathbf{x})$ which are functions of just four variables instead of the seven of the kinetic distribution function. The fluid equations can be derived by taking moments of the Fokker-Planck equation. If Eq. 3.2 is multiplied by 1, $m\mathbf{v}$ and $\frac{1}{2}mv^2$ and integrated in velocity space, the result is the continuity equation, the equation of motion, and the energy equation, respectively. The continuity equation

describes the evolution of the density and is given by

$$\frac{\partial n}{\partial t} = -\nabla \cdot (n\mathbf{u}).$$

The fluid equation of motion describes the evolution of momentum,

$$\frac{\partial}{\partial t} mn\mathbf{u} = en(\mathbf{E} + \mathbf{u} \times \mathbf{B}) - \nabla \cdot \mathbf{P} + \mathbf{F},$$

where $\mathbf{F}$ is the friction force, given by $\mathbf{F} = \int m\mathbf{v}Cd^3v$ where C is the collision operator and $\mathbf{P} = \int m\mathbf{v}\mathbf{v}fd^3v$ is the pressure tensor. The energy equation, describes the evolution of pressure,

$$\frac{\partial}{\partial t}\left(\frac{3}{2}p + \frac{1}{2}mn\mathbf{u}^2\right) + \nabla \cdot \mathbf{Q} = W + \mathbf{u} \cdot (\mathbf{F} + en\mathbf{E}),$$

where $\mathbf{Q} = \int \frac{1}{2}mv^2\mathbf{v}fd^3v$ is the energy flux and $W = \int \frac{1}{2}m(\mathbf{v} - \mathbf{u})^2 Cd^3v$ is the energy exchange [32]. The evolution of the energy flux is then obtained by taking one further moment of Eq. 3.2, and so on. This procedure will not lead to a closed set of equations and the resulting hierarchy must be truncated.

3.2.1 The Extended Drift Wave Model (EDWM)

The Extended Drift Wave Model (EDWM) [33], an extended version of the Weiland model [34], is used in Paper D. Here, the low frequency ($\omega \ll \omega_c$) version of the Braginskii transport equations [35] are used. Following [36], the parallel ion motion for species j is given by

$$m_j n_j \frac{\partial u_{\parallel,j}}{\partial t} = -eZ_j n_j \left[\nabla_\parallel \phi + \frac{1}{c}\left(\frac{\partial A_\parallel}{\partial t} - (\mathbf{u}_{*j} \times \mathbf{B}_\perp) \cdot \hat{\mathbf{b}}\right)\right] - \nabla_\parallel (n_j T_j)$$

where the perpendicular component of the magnetic field is given by $B_\perp = \nabla \times (A_\parallel \hat{\mathbf{b}}) \approx \nabla A_\parallel \times \hat{\mathbf{b}}$, and $\hat{\mathbf{b}} = \mathbf{B}/B$. Here, $u_\parallel$ and $A_\parallel$ are the components parallel to the magnetic field of the fluid velocity and the magnetic vector potential. The hierarchy is truncated at the diamagnetic ion heat flow, $\mathbf{q}_{*j}$, in the ion energy balance equation:

$$\frac{3}{2}n_j\left(\frac{\partial}{\partial t} + \mathbf{u}_j \cdot \nabla\right) T_j + n_j T_j \nabla \cdot \mathbf{u}_j = -\nabla \cdot \mathbf{q}_{*,j} = \frac{5}{2} n_j (\mathbf{u}_{*,j} - \mathbf{v}_{D,j}) \cdot \nabla T_j.$$

The fluid velocities above are $\mathbf{u}_j = \mathbf{u}_\mathbf{E} + \mathbf{u}_{*,j} + \mathbf{u}_{P,j} + \mathbf{u}_{\pi,j} + \hat{\mathbf{b}} u_{\parallel,j}$ where

$$\mathbf{u}_E = \frac{\mathbf{E} \times \hat{\mathbf{b}}}{B}$$

is the $\mathbf{E} \times \mathbf{B}$-drift as discussed earlier,

$$\mathbf{u}_{*,j} = \frac{\hat{\mathbf{b}} \times \nabla(n_j T_j)}{Z_j e n_j B}$$

is the diamagnetic drift which is a purely fluid drift. It arises since in a given volume element more ions gyrating in the magnetic field will be moving in $\hat{\mathbf{b}} \times \nabla n$ direction than the opposite when there is a density gradient, even if the guiding centres are stationary. The polarization drift is given by

$$\mathbf{u}_{P,j} = \frac{d\mathbf{E}}{dt}/(B\omega_{c,j})$$

and

$$\mathbf{u}_{\pi,j} = \frac{\hat{\mathbf{b}} \times \nabla \cdot \pi_j}{Z_j e n_j B}$$

is the drift due to offdiagonal elements of the stress tensor. Furthermore, the drift due to ∇B and curvature, $\mathbf{u}_{D,j}$, is given by

$$\mathbf{u}_{D,j} = \frac{T_j}{m_j \omega_{c,j}} \hat{\mathbf{b}} \times \left(\frac{\nabla B}{B} + \hat{\mathbf{b}} \cdot \nabla \hat{\mathbf{b}} \right). \tag{3.3}$$

The continuity and energy equations for the trapped electrons are similarly derived from a kinetic equation and include the effect from electron-ion collisions. In the electrostatic case the passing electrons are assumed to be Boltzmann distributed. The parallel wave number $k_\parallel$, the perpendicular wave number $k_\perp$, and the magnetic drift frequency $\omega_{D,j}$ are replaced by averages over either a strongly or weakly ballooning eigenfunction. The strongly ballooning eigenfunction is given by $\phi = (1/\sqrt{3\pi})(1 + \cos\theta)$. In weakly ballooning cases a general mode width can instead be used, $\phi \propto \exp(-\alpha\theta^2)$ [37], where the coefficient α is chosen by asymptotic matching for large θ. By linearising the equations and assuming quasineutrality to relate the density perturbations of the species, a dispersion equation is obtained that is formulated as a generalized eigenvalue problem, $\mathrm{A}\mathbf{x} = \omega \mathrm{B}\mathbf{x}$. The α coefficient for the weekly ballooning eigenfunction will be proportional to the growth rate, hence the resulting eigenvalue problem must be solved iteratively in this case. Once the eigenvalues, $\omega = \omega_r + \mathrm{i}\gamma$, where ω_r is the real frequency and γ is the growth rate, of the linear instabilities are obtained a saturation level is estimated by assuming that linear growth is balanced with the nonlinearity [34],

$$\frac{e\tilde{\phi}}{T_e} \approx \frac{1}{k_x \rho_s} \frac{\gamma}{k_y c_s}.$$

In EDWM an extended wave length spectrum and an arbitrary number of ion species can be used. The model is orders of magnitudes more computationally efficient than quasilinear kinetic approaches, and while it includes electromagnetic effects and electron-ion collisions it excludes kinetic resonances that can be important [34].

3.3 Neoclassical transport

Classical transport is the irreducible transport due to collisions. If the effects of a toroidal geometry are added, the transport is known as neoclassical. From

Ohm's law $\mathbf{E} + \mathbf{v} \times \mathbf{B} = \eta \mathbf{j}$, where η is the resistivity tensor with the value $\eta_\parallel$ for the current parallel to the magnetic field and $\eta_\perp$ perpendicular, and the pressure balance equation $\mathbf{j} \times \mathbf{B} = \nabla P$ from single-fluid MHD theory, the velocity perpendicular to the magnetic field can be derived as

$$\mathbf{v}_\perp = \frac{\mathbf{E} \times \mathbf{B}}{B^2} - \eta_\perp \frac{\nabla p}{B^2}. \tag{3.4}$$

With constant temperature and zero electric field, the flux will be $\Gamma_\perp = n\mathbf{v}_\perp = -\frac{\eta_\perp \beta}{2\mu_0} \nabla n$ where $\beta = \frac{nT}{B^2/2\mu_0}$ is the ratio of pressure to the magnetic pressure. The diffusion coefficient is then, from Fick's law which relates the collisional flux to the density gradient,

$$\Gamma = -D \nabla n,$$

$D_\perp = \frac{\eta_\perp \beta}{2\mu_0}$, the classical diffusion coefficient for a fully ionized gas. A rough estimate for the resistivity is obtained if the electron collision time is assumed to be the same as the time for the momentum loss of the electrons when they collide with ions. The force due to the electric field is then balanced by the force due to collisions $Ee = \frac{m_e v}{\tau_e}$. The resistivity is defined by Ohm's law, $E = \eta v n e$ so that $\eta = \frac{m_e}{n_e e^2 \tau_e}$. A thorough calculation from the kinetic equation for the electron distribution function yields a result about half as large [3]. With this estimate, the diffusion coefficient will be the same as if the diffusion were due to a random walk with a step size of the Larmor radius, $D \sim \frac{\rho_e^2}{\tau_e}$, where ρ_e is the electron Larmor radius.

The resistive diffusion in a toroidal plasma is more complicated due to a number of effects which depend on the collision frequency. If the collision frequency is low enough, particles trapped on the low field side of the torus will dominate the transport. The particles are trapped by the mirror force resulting from the fact that the magnetic moment of a particle is constant and that there will be a parallel force on a diamagnetic particle deaccelerating it while going towards higher magnetic field strengths. The particles will then execute banana orbits, so-called since they will trace out banana shaped orbits if viewed in a poloidal cross section. An estimate for the associated diffusion coefficient is then given by a random walk with a step length the same as the width of a banana orbit, given by $w_{be} \sim (q/\varepsilon^{1/2})\rho_e$ where ε is the inverse aspect ratio of the magnetic surface, $\varepsilon = r/R_0$. Since just a fraction of the particles $\sim \varepsilon^{1/2}$ will be trapped, the diffusion coefficient is given by $D \sim \frac{q^2}{\varepsilon^{3/2}} \frac{\rho^2}{\tau_e}$. In this banana regime, the inductive toroidal electric field will also give rise to a new inward flux, the so-called Ware pinch. The electric field will will displace the trapped particle orbit poloidally. Because of this, the ∇B and curvature drifts will not be symmetric about the midplane and the particles will experience an inward drift for longer than they experience an outward drift. The net pinch of the trapped particles is $\langle v_r \rangle \backsimeq -E_\parallel / B_\theta$, independent of charge or mass. Since the trapped particle fraction is $\sim \varepsilon^{1/2}$, the net radial flow goes as [38]

$$\Gamma_r^{Ware} \sim -\varepsilon^{1/2} \frac{E_\parallel}{B_\theta}.$$

If the collisionality is higher, trapping of particles on the low field side will be negligible. Pfirsch-Schlüter diffusion will then be important. It is a result of the outward hoop force that arises due to the toroidal geometry of the plasma. A vertical current is then needed to balance this force. The current is returned by flowing along the magnetic field lines, this is the so-called Pfirsch-Schlüter current [3]. From Eq. 3.4 it is evident that this current will give rise to a perpendicular flow through the parallel electric field $E_\parallel = \eta_\parallel \mathbf{j}_\parallel$. While the fluxes of energy and main ions due to neoclassical effects are typically negligible compared to the turbulent transport, it can have an important effect on heavy impurities, especially if their distribution is poloidally asymmetric [39].

3.4 Turbulent transport and microinstabilities

The class of instabilities which have a wave length not much larger than the ion Larmor radius are called microinstabilities. This type of instabilities does not interrupt the discharge, like larger scale magnetohydrodynamic (MHD) instabilities might do, but the small scale random advection they cause will impact plasma confinement. There are many types of microinstabilities, both electrostatic and electromagnetic. They will create fluctuations in the electric field and thus produce an $\mathbf{E} \times \mathbf{B}$ drift velocity according to $\delta v_\perp = \frac{\delta E}{B}$. If there is also a density fluctuation that is not completely out of phase with $\delta v_\perp$ there will be a convective particle flux through

$$\Gamma_j = \langle \delta v_{\perp,j} \delta n_j \rangle ,$$

where the average is over a flux surface. If the turbulence is electromagnetic and thus also gives rise to fluctuations in the magnetic field, $\delta \mathbf{B}$, that also causes a radial particle flux given by

$$\Gamma_j^{em} = \frac{n}{B_0} \langle \delta v_{\parallel,j} \delta B_r \rangle .$$

This turbulent transport can in the models be described in terms of effective diffusivity and pinches when averaging over time and space. The particle flux can be divided into different terms depending on different driving gradients. For the particle flux we get

$$\frac{R\Gamma_j}{n_j} = D_j \frac{R}{L_{n_j}} + D_{T_j} \frac{R}{L_{T_j}} + D_u \frac{R}{L_u} + RV_{p,j}, \tag{3.5}$$

here R is the major radius of the tokamak, and R/L_{X_j} is the normalized inverse gradient scale length of the quantity X. The first term on the right hand side is ordinary diffusion. The second is thermodiffusion and the third roto-diffusion. $V_{p,j}$ is the convective velocity of species j which is due to parallel compressibility and curvature and ∇B drifts [40]. Impurities with low concentration, trace impurities, will not affect the over-all turbulence. Hence, the impurity gradients

will not affect the impurity diffusion coefficients or the pinch velocity, so Eq. 3.5 will be linear. The signs of the terms in Eq. 3.5 will depend on the dominant instability. In the toroidal ITG/TE branch, as discussed in Section 3.4.1.1, for the electrons the thermodiffusion term will be inwards if the ITG mode is dominant, and outwards if the TE mode is dominant (opposite for impurities), while the pure convection term is typically inwards for both instabilities [41].

Of great importance is the steady state density gradients of main ion and impurities since they determine, for example, whether impurities will be accumulated in the core. If the last three terms in Eq. 3.5 are collected into a total pinch V_j and the equation solved for zero particle flux, i.e. with no sources or sinks of particles other than at the edge, the definition of the so-called peaking factor is obtained,

$$PF_j = \frac{R}{L_{n_j}} = -\frac{RV_j}{D_j}. \tag{3.6}$$

This is the steady state density gradient of zero particle flux for species j. A positive peaking factor means that the density profile is peaked, hence the name, necessitating an inward net particle pinch. Conversely, if the peaking factor is negative, there is a net outward pinch, which is desirable for impurities. Similarly, the electrostatic turbulent radial heat transport is given by

$$Q_j = \frac{3}{2} \left\langle \delta v_{\perp,j} \delta p_j \right\rangle .$$

And the heat transport due to the fluctuations in the magnetic field is given by

$$Q_j^{em} = \frac{1}{B_0} \left\langle \delta q_{\parallel,j} \delta B_r \right\rangle$$

where $q_{\parallel,j}$ is the heat flux for species j parallel to the magnetic field.

The instabilities are characterized by the critical gradients in density and temperature over which they are destabilized. Small fluctuations can often be assumed in the core of the plasma, $\frac{\delta n}{\langle n \rangle} \ll 1$, so the system of equations describing the plasma can be linearised with i.e. $n = \langle n \rangle + \delta n$ and a Fourier description used for the modes $\delta n \sim \exp i(\mathbf{k} \cdot \mathbf{r} - \omega t)$. A dispersion relation relating the wave vector $\mathbf{k}$ to the frequency $\omega = \omega_r + \gamma$, where ω_r is the real frequency and γ the growth rate, can then be obtained. The critical gradient thresholds can then be determined for when the mode is unstable, $\gamma > 0$. These instabilities will grow until they are large enough so that the linear assumptions will not hold, at which point the different modes will couple to each other and enter into the non-linear regime. A saturation amplitude of the fluctuations then needs to be determined in order to calculate the level of transport.

It has been observed that the fluctuations in magnetically confined high-temperature plasmas are typically broadband ($\Delta\omega \sim \omega$) with frequencies and wave lengths similar to those of drift-wave theories, $\omega = \omega_*$, where $\omega_* = \mathbf{k} \cdot \mathbf{v}_*$ is the diamagnetic drift frequency. With typical fusion plasma parameters $\omega_*/\omega_c \sim 10^{-3}$. The turbulent diffusion coefficient from a random walk argument is $D \sim \frac{(\Delta r)^2}{\Delta t} \sim \frac{\Delta\omega}{k_r^2} \sim \frac{\omega_*}{k_r^2}$. If the wave length is similar to the ion

gyroradius $k_r \propto 1/\rho_i$, the gyro-Bohm scaling is obtained, $D \sim \chi \sim \frac{\rho_i}{L}\frac{T}{eB}$. The perpendicular scale length of the microinstabilities are on the order of several gyroradii as the average amplitude of the fluctuation seen by a particle would be averaged out as the scale length approaches the Larmor radius. Zonal flows are an important saturating mechanism, they are discussed in Section 3.4.2.

3.4.1 Drift waves

Drift instabilities are often said to be the cause of the anomalous transport in tokamaks. They are electrostatic and are driven by the free energy in density and electron temperature. They develop from the electron drift wave which can propagate in a plasma slab with a shearless, uniform magnetic field. A wave travelling in the y (poloidal) direction, $\delta n \exp i(k_y y - \omega t)$, has a surface of constant density as indicated in Figure 3.1. Because of the high speed and low inertia of the electrons, a common approximation is to say that they are free to move along the field lines. The force balance will be given by $ne\mathbf{E}_{\|} + \nabla p_e = 0$ which linearised leads to the Boltzmann response for the electron density,

$$\frac{\delta n_e}{n_e} = \frac{e\delta\varphi}{T_e}. \tag{3.7}$$

Thus, a perturbed density will lead to a perturbed electrostatic potential and there will be an electric field pointed from the area of increased density to the area of decreased density. This will cause an $\mathbf{E}\times\mathbf{B}$ drift that will serve to increase the density in less dense regions and increase it in more dense areas, thus causing the density and potential perturbations to oscillate. This wave, the drift wave, will travel in the y direction. By using the quasineutrality condition $\delta n_e = \delta n_i$ and the linearised continuity equation for the ions $\mathrm{i}\omega\delta n_i = \delta v_{\mathbf{E}\times\mathbf{B}}\frac{dn}{dx}$ where the $\mathbf{E}\times\mathbf{B}$ velocity is given by $\delta v_{\mathbf{E}\times\mathbf{B}} = -\frac{1}{B}\frac{\partial\delta\varphi}{\partial y}$ the frequency becomes

$$\omega = -\frac{k_y T_e}{eBn}\frac{\mathrm{d}n}{\mathrm{d}r},$$

which is the electron diamagnetic frequency, ω_{*e}.

Since the density and potential perturbations are in phase, this will not lead to any net transport across the flux surfaces. For that, electron dissipation needs to be introduced through collisions or Landau damping. However, some modes, like the ITG mode, are reactive instead of dissipative and do not require dissipation in order to grow. As discussed in Section 3.3, particles in a tokamak can be either trapped on the low field side or passing, giving rise to different dynamics and modes. Depending on whether it is the parallel motion of passing particles, the magnetic drift of the passing particles or the toroidal procession of the trapped particles that are important for the wave-particle resonance that help drive the instability, they are categorized into slab modes, toroidal modes or trapped particle modes, respectively [42]. Two of the most important electrostatic modes are discussed in the following sections.

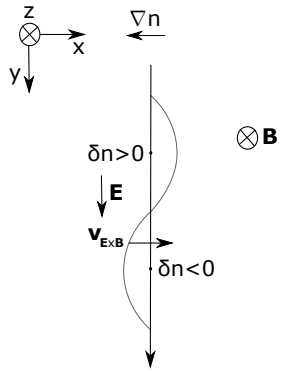

Figure 3.1: Illustration of a drift wave in a slab with a homogeneous magnetic field in the z direction and the wave of constant density travelling in the y (poloidal) direction. Adapted from [3].

3.4.1.1 Ion temperature gradient mode

The ion temperature gradient mode is the most likely driver of ion and electron heat transport in the core of tokamaks [23]. For a qualitative treatment of the ITG mode, trapped particle effects can be neglected, since the frequency of the mode is much larger than that of the ion bounce frequency, $\omega \gg \omega_{b,j}$. An adiabatic Boltzmann electron density response can also be assumed since $k_\parallel v_{Te} \gg \omega \gtrsim k_\parallel v_{Ti}$, however there is no particle or electron heat transport with an adiabatic electron response. The mode is as the name suggest driven by the ion temperature gradient. It is destabilized above a critical value in R/L_{T_i} which depends on plasma parameters. With adiabatic electrons, the critical value increases with the density gradient R/L_n. For this reason, the mode has traditionally been referred to as the η_i mode, η_i being the ratio of the density gradient scale length to the temperature gradient scale length [43]. The spatial scale of the turbulence is on the order of $k_\perp \rho_s \sim 0.1 - 1$ where ρ_s ion acoustic gyroradius. The largest growth rates in linear simulations can typically be found around $k_\perp \rho_s \sim 0.3 - 0.4$ while the peak in the nonlinear flux spectra typically is slightly lower. Two branches can be identified depending on whether the toroidal coupling is important or not. If it is weak, the so-called slab branch can be excited with $\omega \sim (k_\parallel^2 v_{Ti}^2 \omega_{*i} \eta_i)^{1/3}$ [44] where $k_\parallel$ is the component of the wave vector parallel to the magnetic field, v_{Ti} is the thermal velocity of the ions and ω_{*i} is the ion diamagnetic frequency.

In a torus on the low field side, the toroidal branch with $\omega \sim (\eta_i \omega_{*i} \omega_{Di})^{1/2}$, where $\omega_{Di} = \mathbf{k} \cdot \mathbf{v}_{Di}$ is the ion magnetic drift frequency, usually dominates [3]. This is because, in this bad-curvature region, the magnetic field gradient, curvature vector and temperature gradient are all in the same direction. The mechanism behind the bad-curvature driven ITG mode is illustrated in Figure 3.2. A drift wave is set up in the region between the hot and cold plasma.

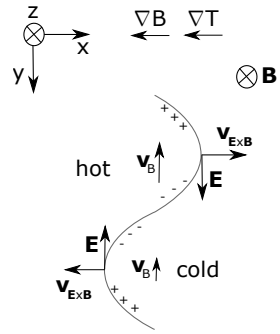

Figure 3.2: The Rosenbluth-Longmire picture of the bad-curvature driven ITG instability [45].

Since the ∇B and curvature drifts are proportional to temperature (Eq. 3.3), the difference in the magnetic drift velocity of the ions will set up an electric field, which will cause an $\mathbf{E} \times \mathbf{B}$ drift that amplifies the original perturbation. The instability is similar to the Rayleigh-Taylor instability, which occur when a lighter fluid is pushing a heavier fluid. An example is when a denser fluid is supported by a less dense fluid under the influence of gravity. On the high field side of the torus the directions of ∇B and ∇T are opposite, so the $\mathbf{E} \times \mathbf{B}$ drift will also be opposite, thus suppressing the original perturbation. Because of this, the perturbations will have their maxima on the outboard side and their minima on the inboard side. Perturbations with this poloidal structure are referred to as ballooning. Following the field lines, the linear eigenfunction of the mode then exhibits a ballooning parity meaning that the real and imaginary part of the perturbed electric potential will be even around $\theta = 0$, where θ is the ballooning angle. An important saturation mechanism for the toroidal ITG mode are the so-called zonal flows, as discussed in Section 3.4.2.

3.4.1.2 Trapped electron mode

Particles that are trapped in the low field region of the torus behave differently than the passing particles in that they average out the parallel velocity over a bounce period. They do not go around the whole torus poloidally, so the curvature drift is not averaged out. This gives rise to several trapped particle modes on the outboard side of the tokamak. One of which is the trapped electron mode. It can be seen as analogous to the ITG mode, but whereas the ions were slow due to inertia in the ITG case, the electrons are now slow due to trapping. The wave number range where the TE mode is destabilized typically overlaps that of the ITG mode.

The collisionality needs to be small enough so that the trapped particles are not scattered into passing orbits. If this is the case, and the ion temperature gradient is small enough so that the ITG mode is not excited, the TE mode

Instability	Source of free energy	Branch	Properties
ITG	∇T_i	Slab	$\omega \leq \omega_{*i}$, $R/L_{T_i} > R/L_{T_i,c}$
		Toroidal	$R/L_{T_i} > R/L_{T_i,c}$
TEM	∇T_e,∇n	Collisionless	$\nu_e < \varepsilon\omega \leq \varepsilon^{3/2} v_{th}/qR$, $L_n q/R < k_\perp \rho_s \leq 1$

Table 3.1: Properties of some microturbulence modes. ω_{*i} is the ion diamagnetic frequency, ρ_s is the ion sound Larmor radius, c_s is the sound speed and L_n is the density scale length. Adapted from [46].

can dominate. The physical picture of the trapped electron mode is that the curvature drift, which is in different directions for ions and electrons, create a charge polarization, resulting in an $\mathbf{E} \times \mathbf{B}$ flow that enhances an initial density perturbation [3]. In contrast to the ITG mode, the trapped electron modes propagate in the direction of the electron diamagnetic frequency. The main drive is the electron temperature and density gradients. Properties of these microturbulence modes are summarized in Table 3.1.

3.4.2 Zonal flows

Zonal flows are $\mathbf{E} \times \mathbf{B}$ plasma flows with $m = n = 0$ where m and n are poloidal and toroidal mode numbers, respectively. They have thus no variation in either the poloidal and toroidal directions and since they are parallel to the flux surfaces they cause no radial heat or particle flux. In the radial direction the associated electric field perturbation varies quickly with a radial scale length similar to to the typical wave number range of the turbulence. Zonal flows are an important saturation mechanism for the ITG mode. The turbulent eddies are sheared by the poloidal flow, so that their radial extent is reduced. They thus reduce the ion heat transport and lead to a higher critical temperature gradient, the so-called Dimits-shift [47]. In low-collisionality plasmas a large portion of the free energy is deposited into zonal flows. They are linearly stable and driven by nonlinear interactions, which transfer energy from the finite-n drift waves to the zonal flows through Reynolds stresses. The energy is then dissipated through collisional processes. In this way, the zonal flows work as a sink for the free energy in the system [48, 42]. Since they are a nonlinear phenomenon, zonal flows are difficult to include in quasilinear transport models, though ad-hoc methods exist [49].

3.4.3 The isotope effect

In several tokamaks an improvement in confinement going from lower to higher hydrogen isotope masses have been observed [50, 51, 52]. This is in contrast to the gyro-Bohm scaling on turbulent transport which predicts that the ion heat flux increases with the square root of the ion mass. This can intuitively

be understood since the step size of a diffusive process which scales with the Larmor radius increases with mass. This inconsistency has been called the isotope effect. Several explanations have been proposed, such as stronger zonal flows with heavier isotopes which reduces the turbulent transport [53]. In gyrokinetic modelling the effect from zonal flows have been shown to reduce the heat fluxes compared to the gyro-Bohm scaling for typical tokamak parameters [54]. For an ITER scenario extrapolated from JET the interaction between $\mathbf{E} \times \mathbf{B}$ shear, zonal flows, magnetic geometry and electromagnetic effects has been shown to play a role in the explanation of the isotope effect on the particle and heat fluxes [55]. The possibility of a deviation from the gyro-Bohm scaling in a pellet fuelled JET discharge is studied in paper C.

Chapter 4

Gyrokinetic theory

The basis of gyrokinetic theory is the assumption that the particles' gyromotion around the magnetic field lines is much faster than the frequencies of the electrostatic or electromagnetic fluctuations of interest. This fast orbital motion can then be averaged over and instead of following the trajectories of the particles, the trajectories of the resulting "charged rings" are followed. Any dependence of the gyroangle, θ, can then be removed. In that way, the number of dimensions is reduced by one and the timestep can be increased past the gyroperiod, which greatly reduces the computational cost.

Nonlinear gyrokinetic simulations are important in the study of low-frequency plasma turbulence and its transport and can be used to simulate a number of instabilities such as the aforementioned ITG and TE modes as well as the trapped ion mode, electron temperature gradient mode, drift-Alfvén turbulence, microtearing and drift-tearing mode and energetic particle driven MHD instabilities [56].

The derivation of the gyrokinetic Vlasov-Maxwell equations relies on the existence of small ordering parameters. The Larmor radius needs to be small compared to the scale lengths of the background magnetic field, L_B, and gradient scale lengths of the background density and temperature, $\epsilon_B = \rho_i / L_B \ll 1$. Furthermore, the cyclotron frequencies need to be much larger than the frequencies of the turbulent fluctuations, $\frac{\omega}{\omega_c} \sim \epsilon_\omega \ll 1$. The wave length of the turbulence cannot be assumed to be large compared to the Larmor radius and full finite-Larmor-radius effects must be retained so that strong wave-particle interactions are captured, $|\mathbf{k}_\perp| \rho_i = \epsilon_\perp \sim 1$. This requirement does not exist for so-called drift-kinetic theories. The fast motion of particles along the field lines compared to the drift velocity across field lines means that the parallel wave length of the turbulence is much larger than the perpendicular ditto, $\frac{|k_\parallel|}{|\mathbf{k}_\perp|} \sim \frac{\epsilon_\omega}{\epsilon_\perp}$. Furthermore, the amplitude ordering parameter ϵ_δ dictates that the amplitude of the fluctuating part of the distribution function, electric, and magnetic field must be small, $\left|\frac{\delta f}{F}\right| \sim \frac{|\delta \mathbf{B}|}{B} \sim \epsilon_\delta \ll 1$. This implies that the energy associated

with the turbulence is small compared to the thermal energy, $\frac{e\delta\phi}{T} \sim \epsilon_\delta$. The ordering parameters for the background, the fluctuating fields and the amplitude are often comparable in practice [56] ($\epsilon_B \sim \epsilon_\omega \sim \epsilon_\delta \sim 10^{-3}$), giving the gyrokinetic ordering

$$\epsilon \sim \frac{\rho_i}{L_B} \sim \frac{\rho_i}{L_F} \sim \frac{\omega}{\omega_c} \sim \frac{k_\parallel}{k_\perp} \sim \frac{e\delta\phi}{T} \ll 1.$$

Instead of studying the evolution of the distribution function of the particles, $F(t, \mathbf{r}, \mathbf{v})$, the evolution of the gyrocenter distribution in gyrocenter phase space $F(t, \mathbf{X}, v_\parallel, \mu)$, is studied, $\mathbf{X}$ is the gyrocenter position, $v_\parallel$ is the gyrocenter parallel velocity and $\mu = mv_\perp^2/(2B)$ is the magnetic moment. The Vlasov equation (3.1) in these coordinates then becomes

$$\frac{\mathrm{d}F}{\mathrm{d}t} = \frac{\partial F}{\partial t} + \frac{\mathrm{d}\mathbf{X}}{\mathrm{d}t} \cdot \nabla F + \frac{\mathrm{d}v_\parallel}{\mathrm{d}t}\frac{\partial F}{\partial v_\parallel} + \frac{\mathrm{d}\mu}{\mathrm{d}t}\frac{\partial F}{\partial \mu} = 0, \tag{4.1}$$

which states that the gyrocenter Vlasov distribution is constant along a gyrocenter orbit in gyrocenter phase space. The fields are decomposed into their background and fluctuating parts, $\Phi(\mathbf{x}) \to \Phi_0(\mathbf{x}) + \Phi_1(x)$, $\mathbf{A}(\mathbf{x}) \to \mathbf{A}_0(\mathbf{x}) + \mathbf{A}_1(\mathbf{x})$. The $\mathbf{E} \times \mathbf{B}$ drift, ∇B-drift and curvature drift are given in Gaussian units by

$$\begin{aligned}
\mathbf{v}_\chi &= -\frac{c}{B_0^2}\nabla\chi_1 \times \mathbf{B}_0 \\
\mathbf{v}_{\nabla\mathbf{B}} &= \frac{\mu}{m\omega_c}\hat{\mathbf{b}}_0 \times \nabla B_0 \\
\mathbf{v}_c &= \frac{v_\parallel^2}{\omega_c}(\nabla \times \hat{\mathbf{b}}_0)_\perp
\end{aligned}$$

where χ_1 is the modified potential $\chi_1 = \bar{\Phi}_1 - \frac{v_\parallel}{c}\bar{A}_{1\parallel} + \frac{1}{q}\mu\bar{B}_{1\parallel}$ and where the over-bar denotes gyroaveraging and $\hat{\mathbf{b}}_0$ denote the unit vector pointing in the direction of $\mathbf{B}_0$**.** The gyroaveraging over a gyro-orbit defined by μ is necessary since the particles do not feel the fields at the gyrocentre. The assumption is made that the amplitudes of the perturbed fields are much smaller than the background fields, the equations of motion are then given as

$$\begin{aligned}
\frac{\mathrm{d}\mathbf{X}}{\mathrm{d}t} &= v_\parallel\hat{\mathbf{b}}_0 + \frac{B_0}{B_{0\parallel}^*}(\mathbf{v}_\chi + \mathbf{v}_{\nabla B} + \mathbf{v}_c), \\
\frac{\mathrm{d}v_\parallel}{\mathrm{d}t} &= \left(\frac{\hat{\mathbf{b}}_0}{m} + \frac{B_0}{mv_\parallel B_{0\parallel}^*}(\mathbf{v}_\chi + \mathbf{v}_{\nabla B} + \mathbf{v}_c)\right) \\
&\quad \cdot \left(-q\nabla\bar{\Phi}_1 - \frac{q}{c}\hat{\mathbf{b}}_0\frac{\mathrm{d}\bar{A}_{1\parallel}}{\mathrm{d}t} - \mu\nabla(B_0 + \bar{B}_{1\parallel})\right), \\
\frac{\mathrm{d}\mu}{\mathrm{d}t} &= 0.
\end{aligned}$$

Inserting these into Eq. 4.1, the standard formulation of the gyrokinetic Vlasov equation for species j is obtained, as in [57],

$$\frac{\partial F_j}{\partial t} + \left(v_\parallel \hat{\mathbf{b}}_0 + \frac{B_0}{B_{0\parallel}^*} (\mathbf{v}_\chi + \mathbf{v}_{\nabla B} + \mathbf{v}_c) \right) \cdot \left(\nabla F_j + \frac{1}{m_j v_\parallel} \left(-q_j \nabla \bar{\Phi}_1 - \frac{q_j}{c} \hat{\mathbf{b}}_0 \frac{\mathrm{d}\bar{A}_{1\parallel}}{\mathrm{d}t} - \mu \nabla (B_0 + \bar{B}_{1\parallel}) \right) \frac{\partial F_j}{\partial v_\parallel} \right) = 0 \quad (4.2)$$

where $\mathbf{B}_0^* = \nabla \times (\mathbf{A}_0 + \frac{mc}{q} v_\parallel \hat{\mathbf{b}}_0)$.

The derivation of the gyrokinetic Vlasov equation can be done by a coordinate transform using Lie formalism to guiding-centre coordinates whereby the magnetic moment and gyro-phase angle are decoupled from the 6D phase space coordinates. The gyromotion is then eliminated by the gyro-centre transform whereby the gyromotion of the particles can be integrated out as presented in [56], reducing the problem from 6D to 5D. In much the same way, the gyrokinetic field equations can be derived from Maxwell's equations using the same Lie generators. The gyrokinetic Maxwell equations together with the gyrocenter Vlasov equation then form a complete self-consistent set of equations. Since fast frequencies are removed, quasineutrality can be assumed so that, for a two-species plasma $q_i n_i = e n_e$ holds. Using Lie perturbation theory in this way, conservation of particle number, energy, momentum and entropy can be ensured [42]. So called δf-codes, such as GENE[1] [58, 59] which is used in this work, go one step further and separate the macroscopic evolution of the plasma from the microturbulence, $F_j \to F_{j0} + F_{j1}$ where the perturbed part is small compared to the background, $F_{j1}/F_{j0} \sim \epsilon$, while assuming that the background part is stationary [57]. This reduces the computational effort. It also simplifies the treatment of collision operators. In order to model collisions, a collision operator must be added to the right hand side of Eq. 4.2, as discussed in the next section.

4.1 Collision operators

Even for high temperature fusion plasmas, collisions can play an important role. Ion-ion collisions can damp zonal flows and electron-ion collisions can stabilize the TE mode since electrons are detrapped. Collisionality is also very important for particle transport. For example, the pure convection term is modified by collisionality so that it becomes smaller inward or even outward for the ITG mode, for the TE mode there can instead be an inward contribution [41]. The linearised Landau-Boltzmann operator [60], used in this work, ensures the conservation of particles, momentum and energy at each point in space. Another property of the collision operator is that of Boltzmann's H-theorem

[1] Short for Gyrokinetic Electromagnetic Numerical Experiment

which says that the entropy will increase until it reaches its maximum entropy state, a Maxwellian. The linearised form of the Landau-Boltzmann operator retains these conservation properties [61]. Since the collisions are assumed to be purely binary, the collision operator can be written on the form

$$C_j(F) = \sum_{j'} C(F_j, F_{j'}),$$

so the effect on species j is given by the sum of contributions from collisions with all species j'. For numerical reasons, physical or numerical dissipation is needed in velocity space. In GENE this can be accomplished by using numerical hyperdiffusion, or by using a collision operator. An account on the implementation in GENE can be found in [62].

4.2 Electromagnetic effects

As the pressure grows in relation to the magnetic pressure the ITG mode is stabilized [63, 64], through coupling to Alfvén modes [65]. If β gets large enough, new modes are excited, primarily the Kinetic Ballooning Mode (KBM) [66]. The critical electron β where this happens is typically around 1 %, slightly lower than the limit for large scale magnetohydrodynamic (MHD) instabilities [67]. The real frequency of the KBM mode is positive, i.e. drifting in the ion diamagnetic direction, similar to the ITG mode. It is distinguished by the typically larger real frequencies and growth rates increase strongly with β. Another electromagnetic instability which can be important for electron heat transport is the microtearing mode [68, 61]. In nonlinear simulations, the relative reduction in heat fluxes is even larger than the reduction in growth rates seen in linear simulations. This is due to nonlinear effects such as zonal flows [67, 69]. As discussed in Section 3.4, the magnetic flutter transport due to the fluctuations in the radial component in the magnetic field also gives rise to radial transport. This transport is typically smaller than the effect of β on the ITG mode that serve to lower the transport. In GENE both perpendicular and parallel fluctuations in the magnet field can be included. Fast ions, i.e. ions with significantly higher energies than the bulk plasma as caused by neutral beam injection or the fusion reactions themselves, can modify the electromagnetic effects. They have been shown to stabilize the ITG mode linearly and nonlinearly both through dilution of the main ion species, Shrafranov shift stabilization and electromagnetic stabilization through the suprathermal pressure gradients as defined as

$$\alpha \equiv q^2 \sum_j \beta_j (R/L_{n,j} + R/L_{T,j}),$$

where q is the safety factor, and the sum is over all species j. Nonlinearly it has been shown that it is the last of these effects that dominates [70]. The effect from fast particles in combination with electromagnetic effects in regions of positive density gradients is investigated in paper D.

4.3 Quasilinear theory

Quasilinear theory has a long history [71]. There are several quasilinear models based on fluid approaches, such as EDWM as previously discussed. More recently quasilinear models based on a gyrokinetic approach have also been developed, such as QuaLiKiz [72]. In quasilinear models the underlying equations are first linearised. Since the fluxes are a product of two fluctuating quantities on the form $\delta n_e \propto \exp(-\mathrm{i}(\omega t - \mathbf{k}\cdot\mathbf{x}))$, such as the particle flux given by $\Gamma_e = \mathrm{Re}\,\langle \delta n_e \delta v_{E\times B}\rangle$, the models are called quasilinear. As previously touched upon, linear instabilities arise from the linearised equations. Nonlinear interactions will eventually cause an instability to be saturated which results in the observed turbulent transport. In general, a model for the saturation level is thus needed to acquire the fluxes. In the gyrokinetic part of this work, only ratios of quasilinear fluxes are used, so this problem is avoided. However, there is a feedback loop in which the saturated turbulence can modify the source of the linear instability. The question then remains to what extent the linear properties of the instabilities survive in the saturated state.

Crucially for the particle transport, the cross phase between density and electrostatic potential needs to remain similar. Thus, the quasilinear assumption is that the relative phase and amplitude between $\delta\phi$ and δn for the particle flux, and δp and $\delta\phi$ for the heat flux, as taken from the linearised equations survive in the saturated turbulence. In order to check that the cross phases remain similar in linear and nonlinear simulations, the probability density function of the cross phases in the nonlinear simulations can be computed and compared to the linear cross phases. This has been done for several gyrokinetic codes and both TE and ITG dominated turbulence and found to agree well [73, 74, 75]. However, the agreement breaks down at larger wave numbers. This is connected to the so-called Kubo number, K. The Kubo number is the ratio between the lifetime of a turbulent eddy and the transit time of a test particle around it. A $K < 1$ then means that the particles are not trapped in the field, and hence move stochastically, which is a condition of validity for the quasilinear framework [75]. This has been shown to be true using nonlinear GENE for a range of cases [76]. In this work, a single length scale is studied at a time. In a more general treatment, the wave numbers of the unstable modes would be summed over, which together with the saturated potential from the saturation model would give the fluxes.

Following [41] an expression for the quasilinear particle flux can be derived from the electrostatic gyrokinetic equation in an $\hat{s} - \alpha$ geometry with a Krook collision operator as

$$\Gamma_k = \left\langle \frac{k_y c_s^2}{\omega_{ci}} \int d^3v F_M \right.$$
$$\cdot \frac{(\hat{\gamma}_k + \hat{\nu}_k)[R/L_n + (E/T_e - 3/2)R/L_{Te}] - (\hat{\gamma}_k \hat{\omega}_{G,k} - \hat{\omega}_{r,k}\hat{\nu}_k)}{(\hat{\omega}_{r,k} + \hat{\omega}_{G,k})^2 + (\hat{\gamma}_k + \hat{\nu}_k)^2}$$
$$\left. \cdot J_0(k_\perp \rho_s)^2 \left| \hat{\phi}_k \right|^2 \right\rangle .$$

Here, F_M is the Maxwellian equilibrium distribution, $\hat{\gamma}_k$ and $\hat{\omega}_{r,k}$ are the growth rate and real frequency of the linear unstable mode. All frequencies have been normalized to the fluid perpendicular drift frequency $\omega_{D,k} = k_y \rho_s c_s / R$. Further, $\hat{\nu}_k$ is the collision frequency, E is the kinetic energy of the particle, and $\omega_{G,k} = k_\parallel v_\parallel + \omega_{d,k}$ where $\omega_{d,k}$ is the ∇B and curvature drift frequency. The Krook collision term is used here for its analytical simplicity, and is not the collision term used in the gyrokinetic modelling in this work. From this equation, several of the properties of the particle flux can be understood. We see that the particle flux can be divided into parts proportional to R/L_n and R/L_{Te}, ordinary diffusion and thermodiffusion respectively, as well as a pure convective term that is not proportional to a gradient, as discussed in 3.4. The ordinary diffusion term is always directed outwards for a peaked profile. For the toroidal ($k_\parallel v_\parallel = 0$) branch the pure convection is inwards as long as $\omega_d \propto \cos\theta + (\hat{s}\theta - \alpha \sin\theta)\sin\theta$, where θ is the ballooning angle, is positive. The direction can change if the magnetic shear is negative or the shift in the magnetic axis given by α is large. Since ω_d arises as an effect of the geometry the pure convection is sometimes referred to as the curvature pinch. The effect of collisions on the pure convection is also easily seen. For a positive real frequency, i.e. the ITG mode, the effect will be an outward contribution while it will be inward for the TE mode with negative real frequency.

4.4 Flux tube simulations

The magnetic equilibrium geometry has to be specified in order to solve the system of equations formed by the gyrokinetic Vlasov and Maxwell equations. The equations could be solved for the whole plasma volume, resolving the whole torus, a so-called global simulation, as discussed in the next section. However, the domain can be reduced significantly if a flux tube domain is used. In this approximation, a field line is followed an integer number of poloidal turns around the torus. Since a tokamak, ignoring ripple effects from the external magnets, is axisymmetrical, all variations are sampled after one turn [62]. The simulation box is then a curved and sheared box around a central field line. This limits the simulations to local investigations, the background density and temperature and their radial gradient are taken to be constant across the radial extent. Since they are constant on a flux surface, their parallel

dependence can be neglected. The flux tube approximation is valid as long as the background perpendicular length scales exceed the turbulence correlation lengths and the radial extent of the box is small compared to the machine size. Another way of stating this is that the local approach is valid in the infinite system size limit, $\frac{\rho_i}{a} \to 0$. The magnetic geometry that contain the metric coefficients that determine the shaping of the box are taken as input. In this work analytical geometries such as $\hat{s} - \alpha$ [77] and Miller equilibriums [22] as well as numerical solutions to the Grad-Shafranov equation [78] are used. As touched upon before, the correlation lengths of the turbulence are much longer along, than perpendicular to, the field lines. Consequently, if a grid aligned coordinate system is used, the computational cost can be lowered by 2 - 3 orders of magnitude since the computational grid can be much coarser along the field lines. The coordinates are then the flux label, x, which is perpendicular to the flux surface, the direction parallel to the field lines, z, and the binormal direction, y, which labels the field lines on the flux surface. Since the simulation domain does not cover the whole physical domain, the boundary conditions should be chosen as to minimize the effect of the reduction. In the radial and binormal direction, periodic boundary conditions for the distribution function are suitable, $F(x+L_x, y, z) = F(x, y, z)$, $F(x, y+L_y, z) = F(x, y, z)$, where L_x and L_y are the box sizes in the direction of x and y, respectively. This also ensures that particles and heat are conserved in the simulation box since losses due to radial fluxes are replenished, thus this choice of boundary conditions also allows for arbitrary long simulation times since there will be no profile relaxation. The periodic boundary conditions also allow for a Fourier representation in the perpendicular plane. In the parallel direction, pseudoperiodic conditions need to be used since, for a general safety factor, the ends of the simulation box which are at the same poloidal position, do not coincide toroidally. Since the turbulent fluctuations are largest at the low field side side, the matching of the ends is done on the high field side, in order to reduce the numerical effects of the boundaries [62].

4.5 Global simulations

If the background quantities, such as density and temperature, vary on the same length scale as the turbulence, global simulations are needed. This can happen in smaller tokamaks or in transport barriers or during pellet fuelling, as examined in papers C and D. In this work, simulations referred to as global are radially global, meaning that a large portion of the plasma volume is resolved radially. For non-axisymmetric magnetic geometries such as stellerators or tokamaks where the ripple effects from the toroidal field coils are important, a global model in the toroidal direction can be necessary instead. Global simulations require much larger resolutions in the radial directions, and are thus significantly more computationally expensive. Periodic boundary conditions, as used in flux tube simulations can no longer be used in the radial direction.

This also means that finite differences have to be used instead of the efficient spectral methods, adding to the computational expense. In GENE, Dirichlet (fixed density and temperature) or von Neumann (fixed gradients) boundary conditions can be chosen, a Dirichlet boundary condition is used at the outer radial boundary. For numerical reasons, when using a Dirichlet boundary condition, a Krook damping term is typically used to smooth out the turbulence close to the boundary. This boundary means that particles and heat will be lost in contrast to the periodic boundary used in flux tube simulations. Thus, particle and heat sources are needed. These can be either adaptive to ensure a specific background gradient, or fixed so that the profiles given a certain power input can be predicted. The first option, a so-called gradient driven setup mirrors the flux tube simulation more closely. The second option, on the other hand, is closer to the physical situation in an experiment but can require long simulations times in order for the profiles to relax. Other than relaxing the requirement on the length scale of the turbulence compared to the background, global simulations also allow the study of additional physical effects. For example, they allow the interaction of ITG turbulence and neoclassical effects [79, 80]. They are also necessary in order to study turbulence spreading whereby perturbations can travel radially into regions where the drift waves are stable. This cannot be modelled in a flux tube domain where the gradients are constant. The spreading typically causes the mean turbulent fluxes to be lower in global simulations than in local simulations and might explain the transition from gyro-Bohm like turbulence to Bohm like turbulence for smaller tokamaks [81, 82, 83].

4.6 Gyrokinetic simulations using GENE

A number of gyrokinetic codes exist that use either a particle-in-cell approach or solves the gyrokinetic equations on a fixed grid. The GENE code [59, 58], which is used in this work, belongs to the latter group. It solves the normalized Vlasov and field equations on a field aligned grid in order to find the particle distribution functions of the included species $f_j(\mathbf{R}, v_\parallel, \mu, t)$, the electrostatic potential $\phi(\mathbf{x}, t)$, and the parallel components of the magnetic vector potential and magnetic field perturbations, $A_\parallel(\mathbf{x}, t)$ and $B_\parallel(\mathbf{x}, t)$. GENE has been carefully benchmarked against other gyrokinetic codes, both in global and local mode [84, 85]. It is a δf code that can be used both in linear and nonlinear mode. Nonlinear mode is much more computationally expensive since it involves the nonlinear coupling between modes with different length and time scales. Furthermore, it requires transformations back and forth between Fourier and real space, where the computation of the nonlinearity has to be performed.

In linear simulations, the coupling between different modes is ignored and one mode is studied at a time. The transport will thus not saturate, but the growth rate and frequency of the largest unstable mode can be found. Besides the initial value solver used for nonlinear simulations, GENE also features an

eigenvalue solver for linear simulations which can find subdominant modes. Since the perturbed quantities do not saturate, the linear mode cannot be used to find absolute fluxes, though quasilinear estimates can be used, like the so-called mixing length estimate. Stability analysis can also be performed, comparing the growth rates of different modes during different circumstances in order to obtain a qualitative understating of the turbulence. In the linear simulations using the initial value solver, the fluxes will grow exponentially until the eigenvalues have been found to within a specified error. The value of the fluxes is thus not interesting, but the quasilinear ratios, like the particle fluxes given as a ratio of the particle flux over the total heat flux, $\Gamma_j / \sum_j q_j$, can be. They allow us to find the quasilinear peaking factors, thus determining whether the mode contributes to an inward or outward pinch for the species. This is done by finding the density gradient of zero particle flux. For the quasilinear peaking factor of the background species, this has to be done in a scan in density gradient since Eq. 3.6 is not linear in R/L_n. For the trace impurities the peaking factors and the contributions from the diffusion, thermopinch and pure convection, as discussed in Section 3.4, can be found in a single run using test species with different gradients of density and temperature as described in [86]. In linear simulations, the choice of length scale, $k_y \rho_s$ becomes important. Typical choices in this work is either the wave number corresponding to the largest growth rate, typically a poloidal wave number of $k_y \rho_s \sim 0.3$ for ITG dominated discharges, or the wave number corresponding to the largest nonlinear fluxes which is usually a bit lower because of the nonlinear transfer through mode coupling.

In a gyrokinetic investigation, linear scans in the poloidal wave number $k_y \rho_s$ are typically first performed in order to find the dominant modes at the different length scales. However, identifying the mode is not always straight forward. The sign of the real frequency, ω_r is the most readily available indicator. Typically, for $k_y \rho_s \lesssim 1$, a positive sign, meaning that the mode is propagating the ion diamagnetic direction, indicates an ITG mode while a negative sign indicates a TE mode. There are however circumstances under which this is not true. For example, the TE mode when driven by the density gradient can propagate in either direction, then sometimes referred to as the ubiquitous mode [34]. It can also be illuminating to check the parity of the eigenfunction. The ITG and TE modes have ballooning parity meaning that the electrostatic potential is even in the ballooning angle while microtearing modes have a tearing parity, meaning that they are odd with respect to the electrostatic potential [61]. In nonlinear simulations, indications of the dominant mode include the ratio between the ion and electron heat fluxes, as well as the cross phases between the fluctuating quantities, for example the density and electrostatic potential.

The main outputs of GENE are the per species space averaged time traces of the fluxes and other fluctuating quantities such as density and temperatures as well as binary data describing the 3D information about the fields, and moments of the distribution function. For the nonlinear simulations, the saturated phase with fully developed turbulence is the interesting part. The radial flux of

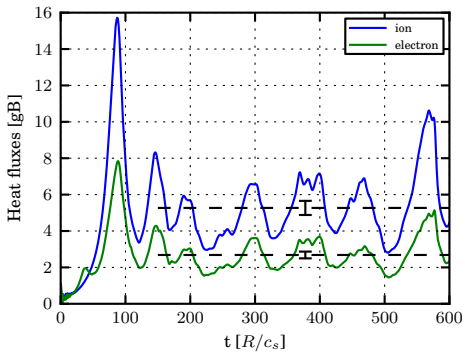

Figure 4.1: Example of time traces of ion and electron heat fluxes for a typical ITG dominated discharge. The time window used along with the obtained mean values and standard deviations are also shown. The heat fluxes are given in gyro-Bohm units defined as $Q_{gB} = c_s n_e T_e (\rho_s/R)$ *where* $c_s = \sqrt{T_e/m_i}$ *and* $\rho_s = c_s/\omega_{ci}$*. Similarly, the particle flux gyro-Bohm unit is given by* $\Gamma_{gB} = c_s n_e (\rho_s/R)$*.*

particles and heat are calculated by multiplying the radial component of the $\mathbf{E}\times\mathbf{B}$ velocity with the perturbed density and pressure, respectively, and averaging in space over a flux surface,

$$\mathbf{\Gamma} = \int \mathrm{d}^3 v \, f_1 \mathbf{v}_\chi$$

$$\mathbf{q} = \int \mathrm{d}^3 v \, \frac{1}{2} m v^2 f_1 \mathbf{v}_\chi,$$

where f_1 is the perturbed part of the particle distribution function and $\mathbf{v}_\chi$ is the $\mathbf{E}\times\mathbf{B}$ velocity. The fluxes can furthermore be split into their electrostatic (due to fluctuations in Φ) and electromagnetic components (due to fluctuations in $A_\parallel$ and $B_\parallel$) parts. A typical time trace of ion and electron heat fluxes in an ITG dominated simulation is shown in Figure 4.1. The nonlinear simulations are performed until the time series contain enough data in the saturated phase to obtain good statistics. The transport during the linear phase is then discarded in the calculation of the time averaged quantities. Since GENE allows for dynamic adjustment of the time step, the trapezoidal rule is used to calculate the average. The values in the time series will be correlated and the statistical error of quantity x has to be determined taking the statistical inefficiency, s, into account through $\sigma = \sqrt{\mathrm{Var}(x_i) s/N}$, where N is the number of data points. The statistical inefficiency can be estimated from the decay of the auto-correlation function,

$$\Phi_k = \frac{\langle x_{i+k} x_i \rangle - \langle x_i \rangle^2}{\langle x_i^2 \rangle - \langle x_i \rangle^2},$$

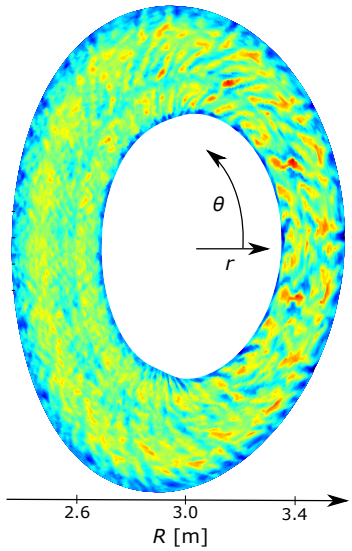

Figure 4.2: Electrostatic fluctuations in a cross section of a plasma. The ballooning structure of the turbulence can be seen, with the largest eddies on the outboard side at $\theta = 0$. This is a simulation of an ITG dominated JET H-mode discharge at mid radius.

as the k where $\Phi_{k=s} = \mathrm{e}^{-2}$ [87].

From the 3D velocity space moments, many important features of the turbulence can be investigated. Contour plots of the fluctuating density or electrostatic potential, as shown in Figure 4.2, can be produced. From contour plots it is possible to tell if there are grid-scale fluctuation which would necessitate more Fourier modes, or turbulent eddies that stretch from boundary to boundary which would require a larger box size. Because of the periodic boundary conditions in local simulations, these eddies can lead to exploding transport. Resolution and box size issues can also be investigated by producing flux spectra and amplitude spectra. In order for the turbulent transport to be well resolved, the flux should tend to zero for low and high $k_y\rho_s$. If not, the box size is too small or the resolution too low, respectively. The amplitude spectra are also checked in order to make sure that the simulation features reasonable spectral decays. While these are necessary requirements in order for the simulation to be considered converged, it is nevertheless often necessary to conduct convergence testing, changing the resolutions and box sizes while verifying that the fluxes remain similar. This adds to the computational cost of nonlinear simulations that are already costly. A typical ITG dominated simulation with finite β effects and non-adiabatic electrons in a flux tube domain requires on the order of 10^5 CPUh. This is only possible on supercomputers. GENE has been shown ta scale well up to 262 144 cores, with a factor 4.6 speedup compared to an ideal factor 8 for large problems. Furthermore, comparing

the heat fluxes to experimental values remains challenging. This is due to the stiff nature of the problem, where the heat flux increases strongly with R/L_T above the nonlinear stability threshold. Together with the uncertainty in the experimental gradients, this often necessities a scaling in temperature gradient to find a realistic heat flux.

Chapter 5

Summary of papers

In **paper A** particle and impurity transport due to ITG/TE mode turbulence was treated selfconsistantly using linear and nonlinear GENE simulations and a more computationally efficient fluid model. Cyclone Base Case parameters were used which correspond to a ITG dominated H-mode discharge. In the self-consistent treatment, the stationary local profiles corresponding to zero particle flux were found simultaneously for the background electrons and the impurities. This is important since the background density gradient can affect the impurity peaking. The background peaking was found to be sensitive to scans over magnetic shear, collisionality, elongation, temperature ratio and plasma β. Thus the self-consistent treatment is important in these cases and was found to mainly enhance the trends from earlier works that assumed a fixed background. However, for collisionality it was found that the increased peaking found for low collisionality was not accompanied by a corresponding increase in impurity peaking, making reactor relevant low collisionality conditions favourable. The fluid, quasilinear GENE and nonlinear GENE background peaking factors were found to be quantitatively comparable and show the same trends, though the quasilinear simulations showed a somewhat higher sensitivity to the scaled parameter. Comparing the quasilinear background and impurity peaking factors, it was found that the impurity peaking factors were consistently lower than the ones for the background, though showed similar scalings. The effect of main ion isotope was also studied and a slight asymmetry in peaking was found between hydrogen, deuterium and tritium. This may result in a D-T fuel separation in cases of high collisionality or large ion to electron temperature ratios.

In **paper B** the attention was turned towards heat transport in JET plasmas. Two matched pairs of ITER-like wall (ILW) and carbon wall (CW) discharges were modelled using GENE in order to investigate the deterioration in global confinement that has been observed since the change in plasma facing components at JET. The discharges were matched with regards to plasma current, the toroidal magnetic field, applied NBI power, average electron density,

safety factor, and triangularity. Linear scans were performed with regards to mismatched dimensionless parameters in the matched pairs. It was found that the relative change in plasma β, Shafranov shift, R/L_{T_e} and magnetic shear served to destabilize the ILW discharges, while the relative change in collisionality and ion to electron temperature ratio serve to stabilize them. The combined effect of the relative changes in these key plasma parameters caused the ITG mode in ILW discharges to be linearly destabilized compared to the matched CW discharges. This was also observed in nonlinear scans over R/L_{T_i} where it was seen that the normalized heat fluxes were larger in the ILW discharges. The ILW discharges also exhibited larger stiffness. Thus, the core confinement in the ILW discharges was affected by the changes in key plasma parameters compared to the CW discharges. However, these parameters are sensitive to the degradation of the edge pedestal that has been observed in ILW baseline H-mode discharges. Hence, it is expected that the core confinement in the ILW discharges would be improved if the edge pedestals were recovered.

The focus was then turned on studying the impact that pellet fuelling has on the heat and particle transport in pellet fuelled plasmas. When the pellets ablate, they temporarily disturb the density and temperature profiles, whereby the microstability properties of the transport are changed, as discussed in Section 2.4. In **paper C** the heat and particle transport in a pellet fuelled JET hydrogen L-mode discharge was analysed using the GENE code. The frequency of the Thomson scattering system, for measuring the profiles, and the pellet injection system were chosen to enhance the time resolution during the pellet ablation time. The discharge was analysed at two time points, at $t = 0.0042\,\mathrm{s}$ after the pellet injection, and at $t = 0.034\,\mathrm{s}$. The first time point corresponds to when the influence from the pellet ablation is the largest and the second to when the profiles have relaxed again. Linear and nonlinear simulations were performed at four radial positions around the pellet ablation peak. Electromagnetic effects and collisions were included, and a realistic geometry used. Since the collisionality was large in this L-mode discharge, collisionless simulations were also run. In the linear analysis it was found that the dominant ITG mode was slightly stabilized on the inside of the pellet ablation peak, where the density gradients are positive, compared to the relaxed intra-pellet time point. In a linear scan of temperature and density gradients it was found that the positive density gradient on the inside of the peak was stabilizing but that this was negated by the increase in temperature gradient caused by the ablating pellet. In the nonlinear simulations the particle fluxes on each side of the peak were of similar magnitudes but in different directions, as shown in Figure 5.1. There was a slight asymmetry with larger fluxes on the outside. The effective diffusion coefficients were reduced on the inside of the peak. In the collisionless case the particle fluxes were larger and the asymmetry increased. The outward ion and electron heat fluxes were greatly reduced at the pellet time point in the positive density gradient region. Since the discharge under study was in hydrogen, simulations were also performed with more reactor relevant deuterium. In units scaled with the species, the fluxes and growth rates were found to be

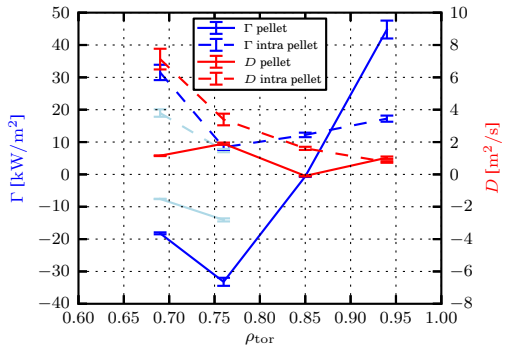

Figure 5.1: Particle fluxes and effective diffusion coefficients at the four radial positions around the density peak.

similar. There was only a small reduction in growth rates with D caused by the collisions. This means that the fluxes follow the gyro-Bohm scaling in this case, $Q_{gB_j} \propto \sqrt{m_j}$, so any improvement in confinement with species mass, the isotope effect as discussed in Section 3.4.3, could not be explained with core transport. In this paper, global simulations in a simplified physical description, electrostatic with adiabatic electrons, were also performed in order to assess whether there were any nonlocal effects caused by the quickly in space varying background density. It was found that the nonlocal effects did not play a major role and that the flux-tube modelling thus is valid for pellet fuelled JET discharges.

In **paper D** the parameter dependence on the particle transport in positive density gradient regions was further investigated using the GENE code and compared to results from the EDWM model for more general tokamak parameters. Here, a circular geometry was used, without collisions and finite β effects, except for scans in these specific parameters. First, the eigenvalues were found in a scan over density gradient and wave number, as shown in Figure 5.2, in order to investigate the dominant modes at the different length scales and R/L_n. For negative R/L_n, corresponding to positive density gradients, the ITG mode was dominant for $k_y\rho_s \lesssim 0.5$ and the TE mode dominant for larger wave numbers. In scans of the collisionality, β, the ion to electron temperature ratio and the magnetic shear, plasma β in particular was found to have a stabilizing effect in the positive density gradient region, lowering the peaking factor and the inward particle flux ratio $\Gamma/(q_i + q_e)$. In order to verify these results, nonlinear GENE simulations were performed in a scan over R/L_n and plasma β, as shown in Figure 5.3. Larger β significantly lowers the inward particle flux in the positive density region in both models. The effects of fast particles, as discussed in Section 4.2, were also studied by including a species with significantly higher temperatures and Maxwellian background dis-

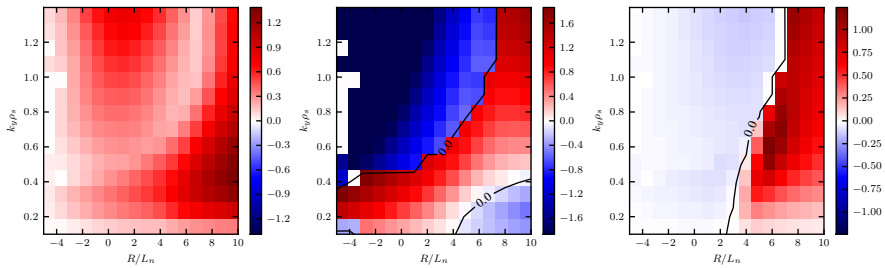

(a) Growth rate in units of c_s/R

(b) Real frequency in units of c_s/R

(c) Normalized particle flux, $\Gamma/\delta n^2$

Figure 5.2: Linear GENE growth rate, real frequency and normalized particle fluxes for typical tokamak parameters in scans over the inverse normalized gradient scale length and normalized poloidal wave number.

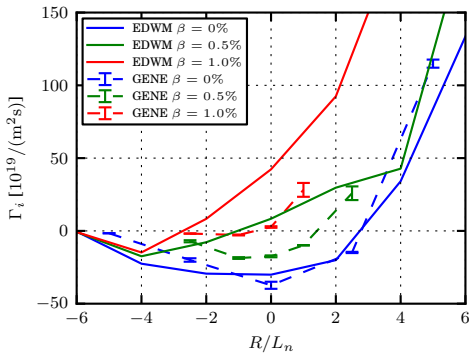

Figure 5.3: GENE and EDWM particle fluxes in a scan over R/L_n and plasma β.

tribution. In nonlinear simulations it was found that with fast particles with sufficiently large temperatures the effective particle diffusion coefficients can be further reduced. A global study of the heat flux in ITG mode turbulence with simplified physics, similar to paper C, was also performed. Here, a peaked Gaussian-like shape was chosen for the logarithmic gradients of temperature and density. While the turbulent transport was lower in the global simulations for positive R/L_n, as expected, the heat flux was increased at small negative R/L_n, suggesting that nonlocal effects can play a subtly different role than usual for a hollow density profile.

Bibliography

[1] DD Clayton. *Principles of stellar evolution and nucleosynthesis*. McGraw-Hill, 1968.

[2] A Grant. Ignition failed: How America's latest attempt at fusion power fizzled. *Science News*, 183:26–29, 2013.

[3] J Wesson. *Tokamaks*, volume 149. Oxford University Press, 2011.

[4] JE Martin. *Physics for Radiation Protection: A Handbook, 2nd Edition, Completely Revised and Enlarged*. Wiley, 2008.

[5] U.S Energy Information Administration. International energy statistics, October 2014.

[6] The secretary-general's advisory group on energy and climate change (EGACC). Energy for a sustainable future - report and recommendations. Technical report, United Nations, 2010.

[7] International Energy Agency. World energy outlook 2013 factsheet. Technical report, International Energy Agency, 2013.

[8] TF Stocker, D Qin, et al. Fifth assessment report of the intergovernmental panel on climate change. Technical report, International Panel on Climate Change, 2013.

[9] PJ Vergragt. How technology could contribute to a sustainable world. *GTI Paper Series*, 28, 2006.

[10] DJC MacKay. *Sustainable Energy - without the hot air*. UIT Cambridge Ltd, 2009.

[11] EG Hertwich, T Gibon, AA Bouman, A Arvesen, S Suh, GA Heath, JD Bergesen, A Ramirez, MI Vega, and L Shi. Integrated life-cycle assessment of electricity-supply scenarios confirms global environmental benefit of low-carbon technologies. *Proceedings of the National Academy of Sciences*, page 201312753, 2014.

[12] V Giordano, F Gangale, et al. Smart grid projects in europe: lessons learned and current developments. Technical report, European Comission Institute for energy, 2011.

[13] OECD. Uranium 2005 - resources, production and demand. Technical report, OECD, 2006.

[14] GC Unruh. Understanding carbon lock-in. *Energy policy*, 28(March):817–830, 2000.

[15] BM Andreev. Separation of hydrogen isotopes in H2O-H2S system. *Separation Science and Technology*, 36:1949–1989, 2001.

[16] U.S. Geological Survey. Minerals commodity summaries 2014. Technical report, U.S. Geological Survey, 2014.

[17] J Ongena and G Van Oost. Energy for future centuries - prospects for fusion power as a future energy source. *Proceedings of the 11th Carolus Magnus summer school on plasma and fusion energy physics*, 2013.

[18] AM Bradshaw, T Hamacher, and U Fischer. Is nuclear fusion a sustainable energy form? *Fusion Engineering and Design*, 86(9-11):2770–2773, October 2011.

[19] FF Chen. *Introduction to Plasma Physics and Controlled Fusion*. Springer, 1984.

[20] K Ikeda. ITER on the road to fusion energy. *Nuclear Fusion*, 50(1):014002, 2010.

[21] H-S Bosch and GM Hale. Improved formulas for fusion cross-sections and thermal reactivities. *Nuclear Fusion*, 32(4):611, 1992.

[22] RL Miller, MS Chu, JM Greene, YR Lin-Liu, and RE Waltz. Noncircular, finite aspect ratio, local equilibrium model. *Physics of Plasmas*, 5(4):973–978, 1998.

[23] EJ Doyle, WA Houlberg, Y Kamada, V Mukhovatov, TH Osborne, A Polevoi, G Bateman, JW Connor, JG Cordey, T Fujita, et al. Plasma confinement and transport. *Nuclear Fusion*, 47(6):S18, 2007.

[24] GF Matthews, M Beurskens, S Brezinsek, M Groth, E Joffrin, A Loving, M Kear, ML Mayoral, R Neu, P Prior, et al. JET ITER-like wall - overview and experimental programme. *Physica Scripta*, 2011(T145):014001, 2011.

[25] S Brezinsek, T Loarer, V Philipps, HG Esser, S Grünhagen, R Smith, R Felton, J Banks, P Belo, A Boboc, et al. Fuel retention studies with the ITER-like wall in JET. *Nuclear Fusion*, 53(8):083023, 2013.

[26] Ph Mertens, JW Coenen, S Devaux, S Jachmich, I Balboa, GF Matthews, V Riccardo, B Sieglin, V Tanchuk, A Terra, et al. Power handling of the bulk tungsten divertor row at JET: First measurements and comparison to the GTM thermal model. *Fusion Engineering and Design*, 88(9):1778–1781, 2013.

[27] MNA Beurskens, J Schweinzer, C Angioni, A Burckhart, CD Challis, I Chapman, R Fischer, J Flanagan, Lorenzo Frassinetti, C Giroud, et al. The effect of a metal wall on confinement in JET and ASDEX Upgrade. *Plasma Physics and Controlled Fusion*, 55(12):124043, 2013.

[28] HT Kim, M Romanelli, I Voitsekhovitch, T Koskela, J Conboy, C Giroud, G Maddison, E Joffrin, et al. Comparative analysis of core heat transport of JET high density H-mode plasmas in carbon wall and ITER-like wall. *Plasma Physics and Controlled Fusion*, 57(6):065002, 2015.

[29] LR Baylor, PB Parks, TC Jernigan, JB Caughman, SK Combs, CR Foust, WA Houlberg, S Maruyama, and DA Rasmussen. Pellet fuelling and control of burning plasmas in ITER. *Nuclear fusion*, 47(5):443, 2007.

[30] SL Milora, WA Houlberg, LL Lengyel, and V Mertens. Pellet fuelling. *Nuclear Fusion*, 35(6):657, 1995.

[31] L Garzotti, J Figueiredo, CM Roach, M Valovič, D Dickinson, G Naylor, M Romanelli, R Scannell, G Szepesi, MAST Team, et al. Microstability analysis of pellet fuelled discharges in MAST. *Plasma Physics and Controlled Fusion*, 56(3):035004, 2014.

[32] RD Hazeltine and JD Meiss. *Plasma confinement*. Courier Corporation, 2003.

[33] PI Strand, G Bateman, A Eriksson, WA Houlberg, AH Kritz, H Nordman, and J Weiland. Comparisons of anomalous and neoclassical contributions to core particle transport in tokamak discharges. In *31th EPS Conference, London 2004, European Physical Society*, volume 28, 2004.

[34] J Weiland. *Collective Modes in Inhomogeneous Plasmas: Kinetic and Advanced Fluid Theory*. CRC Press, 1999.

[35] SI Braginskii. Transport processes in a plasma. *Reviews of plasma physics*, 1:205, 1965.

[36] G Bateman, AH Kritz, JE Kinsey, AJ Redd, and J Weiland. Predicting temperature and density profiles in tokamaks. *Physics of Plasmas*, 5(5):1793–1799, 1998.

[37] J Weiland. Analytical eigenvalue solution for η_i modes of general modewidth. *Physics of Plasmas*, 11(6):3238–3241, 2004.

[38] P Helander and DJ Sigmar. *Collisional transport in magnetized plasmas*, volume 1. Cambridge University Press, 2005.

[39] C Angioni and P Helander. Neoclassical transport of heavy impurities with poloidally asymmetric density distribution in tokamaks. *Plasma Physics and Controlled Fusion*, 56(12):124001, 2014.

[40] C Angioni, AG Peeters, GV Pereverzev, F Ryter, and G Tardini. Theory-based modeling of particle transport in ASDEX Upgrade H-mode plasmas, density peaking, anomalous pinch and collisionality. *Physics of Plasmas*, 10(8):3225–3239, 2003.

[41] C Angioni, E Fable, M Greenwald, M Maslov, AG Peeters, H Takenaga, and H Weisen. Particle transport in tokamak plasmas, theory and experiment. *Plasma Physics and Controlled Fusion*, 51(12):124017, 2009.

[42] X Garbet, Y Idomura, L Villard, and TH Watanabe. Gyrokinetic simulations of turbulent transport. *Nuclear Fusion*, 50(4):043002, 2010.

[43] JW Conner and HR Wilson. Survey of theories of anomalous transport. *Plasma physics and controlled fusion*, 36(5):719, 1994.

[44] J Weiland. *Stability and Transport in Magnetic Confinement Systems*. Springer, 2012.

[45] MN Rosenbluth and CL Longmire. Stability of plasmas confined by magnetic fields. *Annals of Physics*, 1(2):120–140, 1957.

[46] ITER Physics Expert Group on Confinement and Transport and ITER Physics Expert Group on Confinement Modelling and Database and ITER Physics Basis Editors. Chapter 2: Plasma confinement and transport. *Nuclear Fusion*, 39(12):2175, 1999.

[47] AM Dimits, G Bateman, MA Beer, BI Cohen, W Dorland, GW Hammett, C Kim, JE Kinsey, M Kotschenreuther, AH Kritz, et al. Comparisons and physics basis of tokamak transport models and turbulence simulations. *Physics of Plasmas*, 7(3):969–983, 2000.

[48] PH Diamond, SI Itoh, K Itoh, and TS Hahm. Zonal flows in plasma - a review. *Plasma Physics and Controlled Fusion*, 47(5):R35, 2005.

[49] RE Waltz, GM Staebler, W Dorland, GW Hammett, M Kotschenreuther, and JA Konings. A gyro-Landau-fluid transport model. *Physics of Plasmas*, 4(7):2482–2496, 1997.

[50] M Bessenrodt-Weberpals, F Wagner, O Gehre, L Giannone, JV Hofmann, A Kallenbach, K McCormick, V Mertens, HD Murmann, F Ryter, BD Scott, G Siller, FX Soldner, A Stabler, KH Steuer, U Stroth, N Tsois, H Verbeek, and H Zoohm. The isotope effect in ASDEX. *Nuclear Fusion*, 33(8):1205, 1993.

[51] H Urano, T Takizuka, T Fujita, Y Kamada, T Nakano, N Oyama, and the JT-60 Team. Energy confinement of hydrogen and deuterium H-mode plasmas in JT-60U. *Nuclear Fusion*, 52(11):114021, 2012.

[52] H Urano, T Takizuka, N Aiba, M Kikuchi, T Nakano, T Fujita, N Oyama, Y Kamada, N Hayashi, and the JT-60 Team. Hydrogen isotope effects on ITG scale length, pedestal and confinement in JT-60 H-mode plasmas. *Nuclear Fusion*, 53(8):083003, 2013.

[53] TS Hahm, L Wang, WX Wang, ES Yoon, and FX Duthoit. Isotopic dependence of residual zonal flows. *Nuclear Fusion*, 53(7):072002, 2013.

[54] A Bustos, A Bañón Navarro, T Görler, F Jenko, and C Hidalgo. Microturbulence study of the isotope effect. *Physics of Plasmas*, 22(1):012305, 2015.

[55] J Garcia, T Görler, F Jenko, and G Giruzzi. Gyrokinetic nonlinear isotope effects in tokamak plasmas. *Nuclear Fusion*, 57(1):014007, 2016.

[56] AJ Brizard and TS Hahm. Foundations of nonlinear gyrokinetic theory. *Rev. Mod. Phys.*, 79:421–468, Apr 2007.

[57] MJ Pueschel. *Electromagnetic effects in gyrokinetic simulations of plasma turbulence*. PhD thesis, Universität Münster, 2009.

[58] F Jenko, W Dorland, M Kotschenreuther, and BN Rogers. Electron temperature gradient driven turbulence. *Physics of Plasmas*, 7(5):1904–1910, 2000.

[59] The GENE team. The GENE Code. `http://genecode.org/`.

[60] LD Landau. Die kinetische gleichung für den fall coulombscher vechselwirkung. *Phis. Z. Sowietunion*, 10:154–164, 1936.

[61] H Doerk. *Gyrokinetic Simulation of Microtearing Turbulence*. PhD thesis, Faculty of Natural Sciences, Ulm University, 2012.

[62] F Merz. *Gyrokinetic simulation of multimode plasma turbulence*. PhD thesis, Universität Münster, 2009.

[63] J Weiland and A Hirose. Electromagnetic and kinetic effects on the ion temperature gradient mode. *Nuclear Fusion*, 32(1):151, 1992.

[64] F Jenko and W Dorland. Nonlinear electromagnetic gyrokinetic simulations of tokamak plasmas. *Plasma physics and controlled fusion*, 43(12A):A141, 2001.

[65] JY Kim, W Horton, and JQ Dong. Electromagnetic effect on the toroidal ion temperature gradient mode. *Physics of Fluids B: Plasma Physics*, 5(11):4030–4039, 1993.

[66] WM Tang, JW Connor, and RJ Hastie. Kinetic-ballooning-mode theory in general geometry. *Nuclear Fusion*, 20(11):1439, 1980.

[67] MJ Pueschel, M Kammerer, and F Jenko. Gyrokinetic turbulence simulations at high plasma beta. *Physics of Plasmas*, 15(10):102310, 2008.

[68] JF Drake, NT Gladd, CS Liu, and CL Chang. Microtearing modes and anomalous transport in tokamaks. *Physical Review Letters*, 44(15):994, 1980.

[69] J Citrin, J Garcia, T Görler, F Jenko, P Mantica, D Told, C Bourdelle, DR Hatch, GMD Hogeweij, T Johnson, et al. Electromagnetic stabilization of tokamak microturbulence in a high-β regime. *Plasma Physics and Controlled Fusion*, 57(1):014032, 2015.

[70] J Citrin, F Jenko, P Mantica, D Told, C Bourdelle, J Garcia, JW Haverkort, GMD Hogeweij, Thomas Johnson, and MJ Pueschel. Nonlinear stabilization of tokamak microturbulence by fast ions. *Physical review letters*, 111(15):155001, 2013.

[71] AA Vedenov. Quasi-linear plasma theory (theory of a weakly turbulent plasma). *Journal of Nuclear Energy. Part C, Plasma Physics, Accelerators, Thermonuclear Research*, 5(3):169, 1963.

[72] C Bourdelle, X Garbet, F Imbeaux, A Casati, N Dubuit, R Guirlet, and T Parisot. A new gyrokinetic quasilinear transport model applied to particle transport in tokamak plasmas. *Physics of Plasmas*, 14(11):112501, 2007.

[73] T Dannert and F Jenko. Gyrokinetic simulation of collisionless trapped-electron mode turbulence. *Physics of Plasmas*, 12(7):072309, 2005.

[74] F Jenko, T Dannert, and C Angioni. Heat and particle transport in a tokamak: advances in nonlinear gyrokinetics. *Plasma physics and controlled fusion*, 47(12B):B195, 2005.

[75] A Casati, C Bourdelle, X Garbet, F Imbeaux, J Candy, F Clairet, G Dif-Pradalier, G Falchetto, T Gerbaud, V Grandgirard, et al. Validating a quasi-linear transport model versus nonlinear simulations. *Nuclear Fusion*, 49(8):085012, 2009.

[76] J Citrin, C Bourdelle, P Cottier, DF Escande, ÖD Gürcan, DR Hatch, GMD Hogeweij, F Jenko, and MJ Pueschel. Quasilinear transport modelling at low magnetic shear. *Physics of Plasmas*, 19(6):062305, 2012.

[77] JW Connor, RJ Hastie, and JB Taylor. Shear, periodicity, and plasma ballooning modes. *Physical Review Letters*, 40(6):396, 1978.

[78] Gene Development Team. *The Gyrokinetic Plasma Turbulence Code Gene: User Manual*, August 2013.

[79] V Vernay, S Brunner, L Villard, BF McMillan, S Jolliet, TM Tran, and A Bottino. Synergy between ion temperature gradient turbulence and neoclassical processes in global gyrokinetic particle-in-cell simulations. *Phys. Plasmas*, 19(4):042301, 2012.

[80] M Oberparleiter, F Jenko, D Told, H Doerk, and T Görler. Interaction between neoclassical effects and ion temperature gradient turbulence in gradient- and flux-driven gyrokinetic simulations. *Phys Plasmas*, 23(4):042509, apr 2016.

[81] Z Lin, S Ethier, TS Hahm, and WM Tang. Size scaling of turbulent transport in magnetically confined plasmas. *Physical Review Letters*, 88(19):195004, 2002.

[82] L Villard, A Bottino, S Brunner, A Casati, J Chowdhury, T Dannert, R Ganesh, X Garbet, T Görler, V Grandgirard, R Hatzky, Y Idomura, F Jenko, S Jolliet, S Khosh, X Lapillonne, G Latu, BF McMillan, F Merz, Y Sarazin, TM Tran, and T Vernay. Gyrokinetic simulations of turbulent transport: size scaling and chaotic behaviour. *Plasma Phys. Control. Fusion*, 52(12):124038, 2010.

[83] T Görler, X Lapillonne, S Brunner, T Dannert, F Jenko, SK Aghdam, P Marcus, BF McMillan, F Merz, O Sauter, D Told, and L Villard. Flux- and gradient-driven global gyrokinetic simulation of tokamak turbulence. *Phys. Plasmas*, 18(5):056103, 2011.

[84] GL Falchetto, BD Scott, P Angelino, Alessandro Bottino, T Dannert, V Grandgirard, S Janhunen, F Jenko, S Jolliet, A Kendl, et al. The european turbulence code benchmarking effort: turbulence driven by thermal gradients in magnetically confined plasmas. *Plasma Physics and Controlled Fusion*, 50(12):124015, 2008.

[85] X Lapillonne, BF McMillan, T Görler, S Brunner, T Dannert, F Jenko, F Merz, and L Villard. Nonlinear quasisteady state benchmark of global gyrokinetic codes. *Physics of Plasmas*, 17(11):112321, 2010.

[86] A Skyman. *Gyrokinetic simulations of turbulent transport in tokamak plasmas*. Chalmers University of Technology, 2014.

[87] J Thijssen. *Computational physics*. Cambridge university press, 2007.